Downloaded from http://jgs.lyellcollection.org/ at University of St Andrews on February 27, 2015
Journal of the Geological Society, London, Vol. **163**, 2006, pp. 149–164. Printed in Great Britain.

Kinematics of active left-lateral faulting in SE Turkey from offset Pleistocene river gorges: improved constraint on the rate and history of relative motion between the Turkish and Arabian plates

ROB WESTAWAY[1], TUNCER DEMİR[2], ALİ SEYREK[3] & ANTHONY BECK[4]

[1]*Faculty of Mathematics and Computing, The Open University, Eldon House, Gosforth, Newcastle upon Tyne NE3 3PW, UK (e-mail: r.w.c.westaway@ncl.ac.uk)*

[2]*Department of Geography, Harran University, 63300 Şanlıurfa, Turkey*

[3]*Department of Soil Science, Harran University, 63300 Şanlıurfa, Turkey*

[4]*Department of Geography, Durham University, South Road, Durham DH1 3LE, UK*

Abstract: In the Arabian Platform of SE Turkey abundant evidence exists of fluvial incision by *c*. 110 ± 10 m since the late Early Pleistocene, starting in or around marine oxygen isotope stage 22 at 870 ka. This incision, which has accompanied regional surface uplift as the isostatic response to regional erosion, has progressively 'locked' rivers into their gorges in landscape that formerly had much lower relief. We use this effect to estimate 4.44 ± 0.06 km of left-lateral slip on this time scale on the Gölbaşı–Türkoğlu Fault, a segment of the East Anatolian Fault Zone, from offset river gorges, giving a slip rate of 5.10 ± 0.07 mm a^{-1}. Piercing points indicate that this fault has slipped a total of 19 km, making its age 3.73 ± 0.05 Ma. A total of 33 km of relative motion between the Turkish and Arabian plates is documented on this time scale in the vicinity of Gölbaşı, at an overall time-averaged rate of 8.85 ± 0.12 mm a^{-1}, the estimated Euler vector for relative motion between these plates being 0.89 ± 0.01° Ma^{-1} about 33.4°N, 42.3°E. This method can be readily applied to determine slip rates, time-averaged since the late Early Pleistocene, on other strike-slip fault zones worldwide.

The horizontal crustal movements occurring in and around eastern Turkey can be described in terms of mainly strike-slip relative motions between the Eurasian, African, Arabian, and Turkish plates (Fig. 1). The north-trending left-lateral Dead Sea Fault Zone persists northward into the extreme south of Turkey, accommodating the African–Arabian relative motion (Fig. 1). Farther NE, the NE–ENE-trending East Anatolian Fault Zone takes up the Turkish–Arabian relative motion, which is also in the left-lateral sense (Fig. 1). The Dead Sea Fault Zone and East Anatolian Fault Zone are linked by a complex network of active left-lateral faults, whose kinematics are not yet fully understood (Westaway 2004*a*). One of these structures, the Gölbaşı–Türkoğlu Fault, forms the subject of this study.

The Gölbaşı–Türkoğlu Fault is a well-known feature of the active left-lateral faulting regime in SE Turkey (e.g. Arpat & Şaroğlu 1972; McKenzie 1976; Yalçın 1979; Muehlberger 1981; Muehlberger & Gordon 1987; Şaroğlu *et al*. 1992; Westaway 1994, 2003, 2004*a*; Westaway & Arger 1996); it trends ENE–WSW and can be traced for *c*. 70 km between the towns of Gölbaşı and Türkoğlu (Figs 1 and 2). The Westaway (2004*a*) kinematic model has established that a high degree of consistency exists in this region between the geological evidence pertaining to active strike-slip faulting and the crustal velocity field determined by McClusky *et al*. (2000) using the Global Positioning System (GPS). This model predicts Turkish–Arabian relative motion at 8.0 mm a^{-1} towards S48°W around Gölbaşı, accommodated by left-lateral slip at *c*. 4 mm a^{-1} on the Gölbaşı–Türkoğlu Fault and at most *c*. 1 mm a^{-1} on the east–west-striking Sürgü Fault farther north (Fig. 1; total slip estimated as *c*. 4 km by Westaway 2004*a*, based on Perinçek & Kozlu 1983) the remaining *c*. 3–4 mm a^{-1} being taken up on an array of NNE–SSW-striking left-lateral faults farther south (Fig. 2), about which little is currently known. In addition, components of distributed deformation are occurring between some left-lateral faults in this region, which are thus not transform faults. The most significant examples are the northernmost segments of the Dead Sea Fault Zone in western Syria and the extreme south of Turkey (Fig. 1), which become increasingly misaligned, as one moves farther north, with respect to the African–Arabian Euler pole, in the transpressive sense (Westaway 2003, 2004*a*). They thus require significant components of crustal shortening in their surroundings (Westaway 1995), resulting in crustal thickening and surface uplift. They account for much of the local topography of this region (Westaway 2003, 2004*a*).

Superimposed onto these local effects of active faulting is a component of regional uplift, estimated to have had a typical rate of *c*. 0.1 mm a^{-1} during the Mid–Late Pleistocene in parts of the Arabian platform located away from the active faulting (Arger *et al*. 2000; Bridgland *et al*. 2003; Demir *et al*. 2004, 2005). The main evidence for this process is provided by fluvial incision, leading to the widespread development of long time scale depositional river terrace staircases along the River Euphrates (Fig. 2b) and its tributaries (e.g. Ponikarov *et al*. 1967; Besançon & Sanlaville 1981; Erol *et al*. 1987; Tyráček 1987; Minzoni-Deroche & Sanlaville 1988; Wilkinson 1990; Besançon & Geyer 2003; Kuzcuoğlu *et al*. 2004). The chronology of the Euphrates terrace staircase has been established by Besançon & Sanlaville (1981), Minzoni-Deroche & Sanlaville (1988) and Besançon & Geyer (2003) as part of a correlation scheme for the Pleistocene of the surrounding region.

The uplift of this region is regarded as the isostatic consequence of coupling between surface processes (primarily, in this

Downloaded from http://jgs.lyellcollection.org/ at University of St Andrews on February 27, 2015

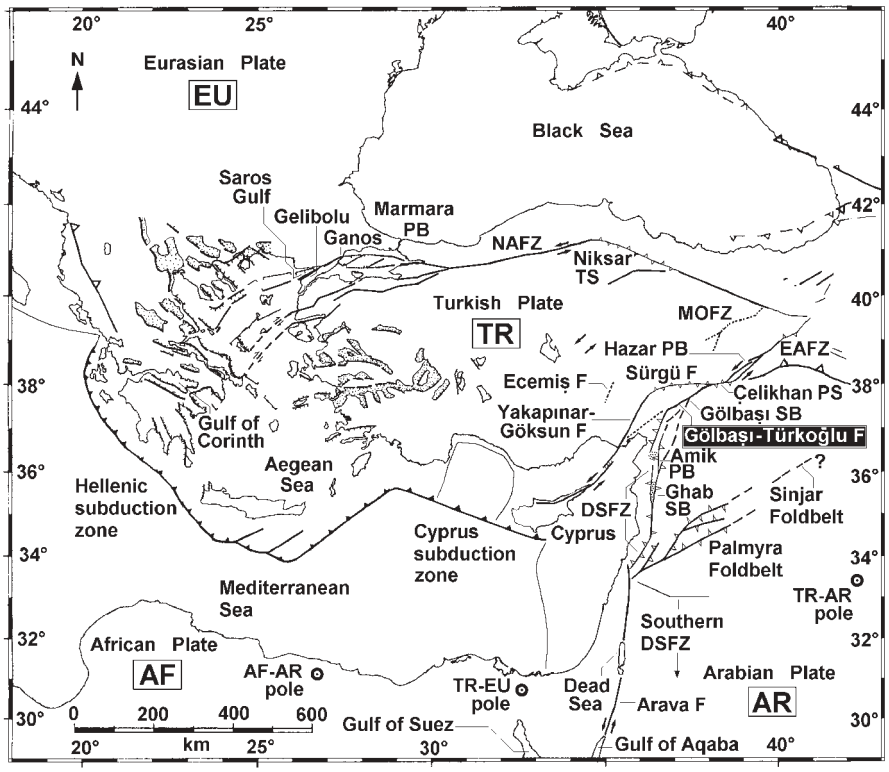

Fig. 1. Map illustrating the plate tectonic context of the present study region, modified from figure 1 of Westaway (2004*a*) that lists original sources of information. DSFZ, Dead Sea Fault Zone; EAFZ, East Anatolian Fault Zone; NAFZ, North Anatolian Fault Zone; MOFZ, Malatya–Ovacık Fault Zone. Structures are classified using abbreviations: F, fault; PB, pull-apart basin; PS, transpressional stepover; SB, splay basin; TS, transtensional stepover. Positions of preferred Euler poles, for the relative motions of the African and Arabian plates (AF–AR; from Klinger *et al*. 2000), the Turkish and Arabian plates (TR–AR; from Westaway 2004*a*), and the Turkish and European plates (TR–EU; from McClusky *et al*. 2000), are labelled. The kinematic model of Westaway (2004*a*) predicted TR–AR relative rotation at 0.7145° Ma^{-1} about a pole at 33.4°N, 42.3°E, roughly concentric to the East Anatolian Fault Zone (and northern Dead Sea Fault Zone), as illustrated. It should be noted that the TR–EU pole is also concentric to almost the whole NAFZ, consistent with right-lateral transform faulting. However, the AF–AR pole is concentric to only the southern Dead Sea Fault Zone: it requires left-lateral transpression, not transform faulting, farther north.

region, erosion) and the induced inward lower-crustal flow (e.g. Arger *et al*. 2000; Westaway 2002*a*, *b*, *c*, 2004*b*; Bridgland *et al*. 2003; Demir *et al*. 2004, 2005; Westaway *et al*. 2004). Numerical modelling (e.g. Westaway 2002*a*; Westaway *et al*. 2004) has established that, following a regional increase in erosion rates, during each time step the inflow of lower crust exceeds the typical thickness of the layer of material that is eroded, causing crustal thickening and thus providing a natural explanation for the observed surface uplift. In many regions the change in global climate that marked the start of *c*. 100 ka Milankovitch cyclicity at marine oxygen isotope stage (MIS) 22 (*c*. 870 ka; e.g. Shackleton *et al*. 1990) is observed to accompany an increase in rates of fluvial incision (e.g. Kukla 1975, 1978; Westaway 2001, 2002*b*, *c*; Bridgland & Westaway 2005*a*, *b*). This effect can be readily explained as a consequence of increased rates of erosion, possibly resulting from reductions in vegetation at times of cold or arid climates, combined with increases in stream power because other parts of each climate cycle (the pluvials of the Mediterranean Pleistocene record) have involved high rainfall (e.g. Rossignol-Strick 1985, 1999; Rohling & Hilgen 1991; Kroon *et al*. 1998; Collier *et al*. 2000). Numerical modelling by Demir *et al*. (2005) confirms that the Euphrates terrace records in SE Turkey, northern Syria, and western Iraq indicate increases in uplift rates following MIS 22, supporting the interpretation originally proposed by Tyráček (1987) for the reach of this river in Iraq, based on the similarity between its record and fluvial terrace staircases in central Europe. This modelling by Demir *et al*. (2005) also confirms a typical value of *c*. 110 m for the uplift indicated since MIS 22 on the reach of the Euphrates in SE Turkey.

The total slip on the Gölbaşı–Türkoğlu Fault has been estimated as *c*. 16 km from the apparent offset of the WSW end of a body of Neotethyan ophiolite east of Türkoğlu (Westaway & Arger 1996; w–w′ in Fig. 2). Its age is estimated as *c*. 4 Ma in the Westaway (2003, 2004*a*) kinematic models; hence the estimated *c*. 4 mm a^{-1} (i.e. *c*. 16 km in *c*. 4 Ma) slip rate. Westaway & Arger (1996) also noted the presence, about halfway between Gölbaşı and Türkoğlu, of three adjacent rivers, the Kısık, Koca and Gök, whose gorges are all offset left-laterally by *c*. 4 km across this fault. They suggested that these gorges may have become 'locked' in their present positions following the regional increase in rates of erosion and uplift during and after MIS 22. The resulting slip rate estimate of *c*. 4.6 mm a^{-1} (*c*. 4 km in 870 ka) is in reasonable agreement with the alternative value derived from the age of and total slip on the Gölbaşı–Türkoğlu Fault. The present study examines these offset river gorges and their surroundings in more detail, testing whether this interpretation is valid, and thus tightens the existing observational constraints on the rate and history of slip on the Gölbaşı–Türkoğlu Fault. If correct, it can form the basis of a method for estimating slip rates on million-year time scales on strike-slip fault zones worldwide.

Observational evidence

Geological background

We adopt the local stratigraphic nomenclature established by Terlemez *et al*. (1997). The oldest rock exposed along the Gölbaşı–Türkoğlu Fault (Fig. 2a) is the Hatay Ophiolite, which was obducted onto the northern margin of the Arabian Platform during the Maastrichtian (*c*. 70 Ma), having apparently formed around 90 Ma at a spreading centre within the adjacent Southern Neotethys Ocean (e.g. Delaloye *et al*. 1977; Delaloye & Wagner

Downloaded from http://jgs.lyellcollection.org/ at University of St Andrews on February 27, 2015

Fig. 2. Maps of the study region and its surroundings, adapted from Westaway & Arger (1996, fig. 3). (**a**) Geological map, simplified from the 1:500 000 scale map by Tolun & Erentöz (1962), showing (with bold arrows and letters) piercing points for estimating slip on left-lateral strike-slip faults from the regional geology. The Late Oligocene and Miocene grouping includes the upper part of the marine carbonate sequence represented by the Midyat Group and the overlying Miocene clastic deposits (i.e. the Şelmo Formation). The grouping 'Metamorphic basement' includes Mesozoic and older metamorphic rocks of the former Anatolian continental fragment, north of the suture of the Southern Neotethys Ocean. (**b**) Topography and drainage, simplified from US National Imagery and Mapping Agency Tactical Pilotage Chart G4-B at 1:500 000 scale, showing contours at 1000 ft intervals (i.e. at 305, 610, 914, 1219, 1524, 1829, 2134 and 2438 m). Ticks indicate downhill sides of contours where unclear. The River Euphrates (Fırat) around Birecik is at *c*. 340 m a.s.l. GTF, Gölbaşı–Türkoğlu Fault; GF, Göksu Fault, the in-line continuation to the ENE of the Gölbaşı–Türkoğlu Fault; EHF, the East Hatay Fault; KOF, Karataş–Osmaniye Fault; KF, Kartal Fault KPF, 'Kırkpınar Fault' (see Westaway & Arger 1996) that is now known to oversimplify the complexity of the NNE–SSW-oriented left-lateral faulting that splays from the Gölbaşı–Türkoğlu Fault in this region (see Westaway 2003, 2004*a*). Other active faults are not shown (see Fig. 1). Locations are indicated for Figures 4, 6 and 8 (in (**b**)) and 9 (in (**a**)).

1984; Al-Riyami *et al*. 2002). Ophiolite obduction was followed unconformably by deposition of the Besni Formation, consisting of multi-coloured conglomerate and sandstone, passing upwards into Middle or Upper Maastrichtian limestone. This is followed by the uppermost Maastrichtian to Palaeocene Germav Formation, consisting of marl and clayey limestone, overlain by the Eocene to Upper Miocene Midyat Group carbonates. Along the Gölbaşı–Türkoğlu Fault, this is typically represented by the Lutetian Hoya Formation, a particularly pure, well-lithified limestone that resists erosion and forms much of the relief of the region.

Mid-Miocene uplift and sea-level fluctuation (e.g. Karig & Kozlu 1990; Arger *et al*. 2000) resulted in the interbedding of fluvial (Şelmo Formation) and shallow marine sediments (e.g. Derman 1999). Contemporanous basaltic andesite volcanism (Arger *et al*. 2000), the 'Yavuzeli Basalt' (Terlemez *et al*. 1997), also occurred, resulting in a complex succession of lava flows interbedded with the sediments (e.g. Derman 1999). K–Ar dating

Downloaded from http://jgs.lyellcollection.org/ at University of St Andrews on February 27, 2015

by Arger *et al*. (2000) established the age of this volcanism as *c*. 16 Ma, consistent with the biostratigraphic age of the associated shallow marine sediments (Karig & Kozlu 1990).

Before this dating study by Arger *et al*. (2000), this volcanism in the Pazarcık–Türkoğlu area was widely thought to be Quaternary (see Westaway & Arger 1996). However, the assumption of a Quaternary age was based on miscorrelation with other Quaternary volcanic fields elsewhere in SE Turkey (Terlemez *et al*. 1997). None the less, a Quaternary age continues to be claimed, and has been used to argue for a young (less than *c*. 2 Ma) age for the initiation of the East Anatolian Fault Zone (e.g. Yürür & Chorowicz 1998; Adıyaman & Chorowicz 2002). However, as dating shows that this volcanism is Miocene, such reasoning should no longer be used (see Yurtmen *et al*. 2002). Likewise, some interpretations (e.g. those by Lyberis *et al*. (1992), Chorowicz *et al*. (1994) and Adıyaman & Chorowicz (2002)) have claimed, largely based on interpretation of satellite imagery without supporting field evidence, that the Gölbaşı–Türkoğlu Fault is a minor structure and the principal active deformation in its vicinity is shortening, leading to the development of the adjacent Ahır anticline (Fig. 2a) and its counterparts. However, our field investigations, like those of Westaway & Arger (1996), reveal no evidence that these anticlines are active. Their folding predates the East Anatolian Fault Zone, justifying the use by Westaway & Arger (1996) and in the present study of offset anticline axes as piercing points to quantify the young strike-slip. Our fieldwork also indicates that the interpretation by Adıyaman & Chorowicz (2002), that the Gölbaşı–Türkoğlu Fault is a normal fault with downthrow to the SSE, is incorrect, as no systematic component of vertical slip can be identified. In some places the topography across this fault is lower on its SSE side, but elsewhere the lower ground is on its NNW side; these local patterns can be readily explained by juxtaposition of different rock types, some more easily erodable than others, as a result of the active left-lateral slip (see Westaway & Arger 1996).

The final stratigraphic unit, the 'Harabe Formation' of Terlemez *et al*. (1997), consists of fluvial gravel, sand and silt. This has been assigned a nominal 'Pliocene' age, as parts of it stratigraphically overlie the Yavuzeli Basalt. However, on the basis of this limited constraint, individual fluvial deposits grouped using this term could have any age from Late Miocene to Mid-Pleistocene. By analogy with the similarly designated 'Asartepe Formation' in western Turkey (see Westaway *et al*. 2004), it may well consist of a complex mixture of stacked fluvial units and inset deposits, forming high river terraces, such that it should arguably not be regarded as a 'Formation' in any meaningful stratigraphic sense.

Fault zone morphology

The Gölbaşı–Türkoğlu Fault can be readily identified for most of its length from the geomorphology. Its eastern end was described in detail by Westaway & Arger (1996). To the best of our knowledge, the only previous detailed investigation of the central and western Gölbaşı–Türkoğlu Fault has been by Yalçın (1979). In the western Gölbaşı Basin the Gölbaşı–Türkoğlu Fault strikes SW and runs for *c*. 10 km along the base of a *c*. 100 m high, NW-facing escarpment on its Arabian side, past Kösüklü, Çatalağaç and Küçükören (Figs 3a and 4). As illustrated in Figure 3a, this escarpment exposes the uppermost Maastrichtian–Palaeocene clayey limestone of the Germav Formation; its base forms the alluvial plain in the basin interior at *c*. 880 m above sea level (a.s.l.), whereas its top truncates a low-relief land surface formed in the Germav Formation, which in places slightly exceeds 1000 m a.s.l (Fig. 4).

The Kısık drainage catchment. About 1 km from the western end of the Gölbaşı Basin, the River Aksu exits it through a gorge in this escarpment (Fig. 4). At the entrance to this gorge (at [CB 6190 6725]) the Aksu is joined by the Kısık, one of its principal tributaries, draining an area of *c*. 40 km^2. From this confluence the Gölbaşı–Türkoğlu Fault follows the Kısık upstream, passing between Sakarkaya and Soku, with a typical S60°W trend (Fig. 4). The local relief is much more dramatic than farther NE, the escarpment on the Turkish side of the Gölbaşı–Türkoğlu Fault rising from *c*. 900 m to *c*. 1300 m a.s.l. as it truncates the axis of the Ahır anticline in Midyat Group limestone (Fig. 2a). Westaway & Arger (1996) located this anticline axis at [CB 5950 6560] (their locality Q; Fig. 2a) and regarded it as conjugate to the axis of the Körkün anticline on the Arabian side of the Gölbaşı–Türkoğlu Fault near the eastern end of the Gölbaşı Basin (their locality T, at [CB 8520 8610]; Fig. 2a). The 33 km offset between these piercing points indicates the total slip on all Late Cenozoic left-lateral strike-slip faults that pass through the Gölbaşı Basin, comprising the Gölbaşı–Türkoğlu Fault and the NNE–SSW-striking fault zone that splays southward from it near the eastern end of this basin (Fig. 2), which is not investigated in the present study.

In contrast, the escarpment on the Arabian side of the Gölbaşı–Türkoğlu Fault maintains a roughly constant *c*. 120 m height, for instance rising from the *c*. 920 m river level to *c*. 1040 m a.s.l. where the Kısık River joins the fault line (Fig. 4). However, moving WSW, the exposure in the face of this escarpment passes down-section, from the Germav Formation into the underlying Besni Formation, recognizable from its distinctive coloration, and then into the Hatay Ophiolite (Fig. 3b). Tolun & Erentöz (1962) mapped the eastern end of outcrop of ophiolite on the Arabian side of the Gölbaşı–Türkoğlu Fault in the vicinity of [PC 5640 6375], *c*. 1 km WSW of the point where the Kısık River reaches the fault line (Y in Fig. 4b). East of this point, beyond the gorge flank on its Arabian side, outliers of the Besni Formation rise to *c*. 1100 m a.s.l. (Fig. 3c). The roughness of the local topography raises the possibility that these might overlie ophiolite, thus concealed beneath scree deposits, which may thus persist as far east as Y′ (Fig. 4b). Furthermore, Figure 3b indicates that ophiolite is also present farther ENE in the escarpment face at least as far as [CB 5900 6550] (Z in Fig. 4b). We return to the issue of how to determine precise piercing points in this ophiolite during discussion of the total slip on the Gölbaşı–Türkoğlu Fault.

At the WSW end of the offset reach of the Kısık River, an offset reach of the Çınarcık tributary follows the line of the Gölbaşı–Türkoğlu Fault for *c*. 2 km. However, this is a minor drainage system compared with the Kısık trunk channel, draining only *c*. 3 km^2 of land area, and has evidently thus been unable to incise in pace with the regional uplift that has occurred. At its confluence with the Kısık it forms a hanging valley, where it cascades down to the level of the Kısık, as illustrated in Figure 3c.

The Koca drainage catchment. Beyond the sector where the Çınarcık follows the line of the Gölbaşı–Türkoğlu Fault, this fault crosses the col, at *c*. 1240 m a.s.l. (at [CB 5540 6340], near Karaağaç Tepe hill (1249 m a.s.l., at [CB 5550 6332]; Fig. 3c), entering the Koca river system (Figs 5a and 6). In this reach this fault typically trends S65°W, the outcrop being ophiolite on its Arabian side and partially lithified Miocene fluvial sand and

Downloaded from http://jgs.lyellcollection.org/ at University of St Andrews on February 27, 2015

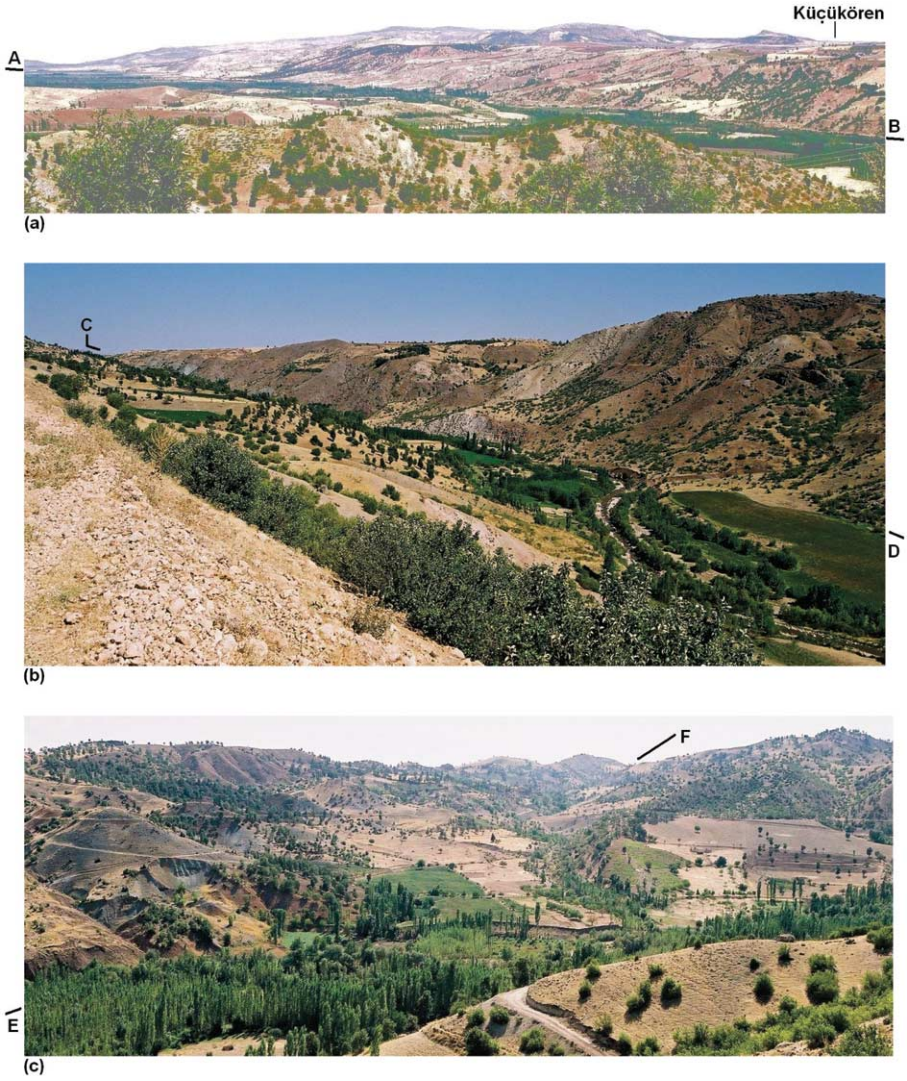

Fig. 3. (**a**) View from [CB 60140 67230], looking N60°E at the linear valley along the Gölbaşı–Türkoğlu Fault at the western end of the Gölbaşı Basin. The Aksu River locally flows ENE–WSW (i.e. from A to B). Küçükören village, on the right above the fault escarpment, is *c*. 970 m a.s.l., *c*. 100 m above river level. The viewpoint is *c*. 1 km SE of Sakarkaya on the road to Kısık village, on the eastern flank of the Sakarkaya anticline (Q in Fig. 2a; part of the larger Ahır anticline) where it is truncated by the Gölbaşı–Türkoğlu Fault. The light colour of the outcrop on the opposite (Arabian) side of the fault indicates clayey limestone of the Germav Formation. (**b**) View eastward along the Gölbaşı–Türkoğlu Fault linear valley (C–D) from [CB 58199 65517]. The Kısık River flows from right to left, with a low terrace visible, *c*. 4 m above present river level. The reddish-brown colour of the rocks on the opposite side of the fault indicates the Besni Formation, in contrast to the white Midyat Group limestone in the foreground. Ophiolite is also visible in the escarpment face opposite (thus, it is used as a piercing point, Z in Table 3, to constrain the total slip on the Gölbaşı–Türkoğlu Fault), although *in situ* exposure there is often poor because of cover by scree deposits. (**c**) View SW from an adjacent point, [CB 58184 65513], showing the confluence between the Kısık River that joins the Gölbaşı–Türkoğlu Fault from the Turkish side and its Çınarcık tributary, which flows ENE along this linear valley. E–F indicates the line of the Gölbaşı–Türkoğlu Fault. On the left, multi-coloured deposits of the Besni Formation are visible down to river level on the Arabian side of the Gölbaşı–Türkoğlu Fault, indicating that the fault is nearby. Similar deposits (which may possibly overlie the ophiolite, concealed beneath scree deposits) can be observed beyond the gorge flank, rising from *c*. 1040 to *c*. 1100 m a.s.l. The conical hill on the skyline is Karaağaç Tepe, which adjoins the Gölbaşı–Türkoğlu Fault on its Arabian side and marks the col bounding the Koca drainage catchment. Co-ordinates of these and other photographs were measured in the field using a handheld GPS receiver and are expressed using the Universal Transverse Mercator (UTM) co-ordinate system.

gravel of the Şelmo Formation on its Turkish side. Although the regional topographic gradient is southward, the more erosion-resistant ophiolite means that locally the land surface is typically higher in the immediate vicinity of the fault on its Arabian side (Fig. 6).

The Gölbaşı–Türkoğlu Fault descends to the level of the Koca River and its principal tributary, the Sincer, along a gulley, passing directly south of Karaağaç village (at [CB 5500 6305]) and crossing the Velikler tributary, which is not significantly offset from the modern outlet gorge of the Sincer across the fault (Fig. 5a), reaching the Sincer at *c*. 905 m a.s.l. It then runs upstream along the Sincer, which is offset left-laterally by *c*. 800 m (Figs 5a and 6), forming a short section of linear valley between ophiolite (on the Arabian side; Gökgedik Tepe, rising to *c*. 1020 m) and Şelmo Formation sand and gravel (on the Turkish side; Orta Sırtı, rising to *c*. 1070 m a.s.l).

Around [CB 5370 6230] the Gölbaşı–Türkoğlu Fault leaves

Downloaded from http://jgs.lyellcollection.org/ at University of St Andrews on February 27, 2015

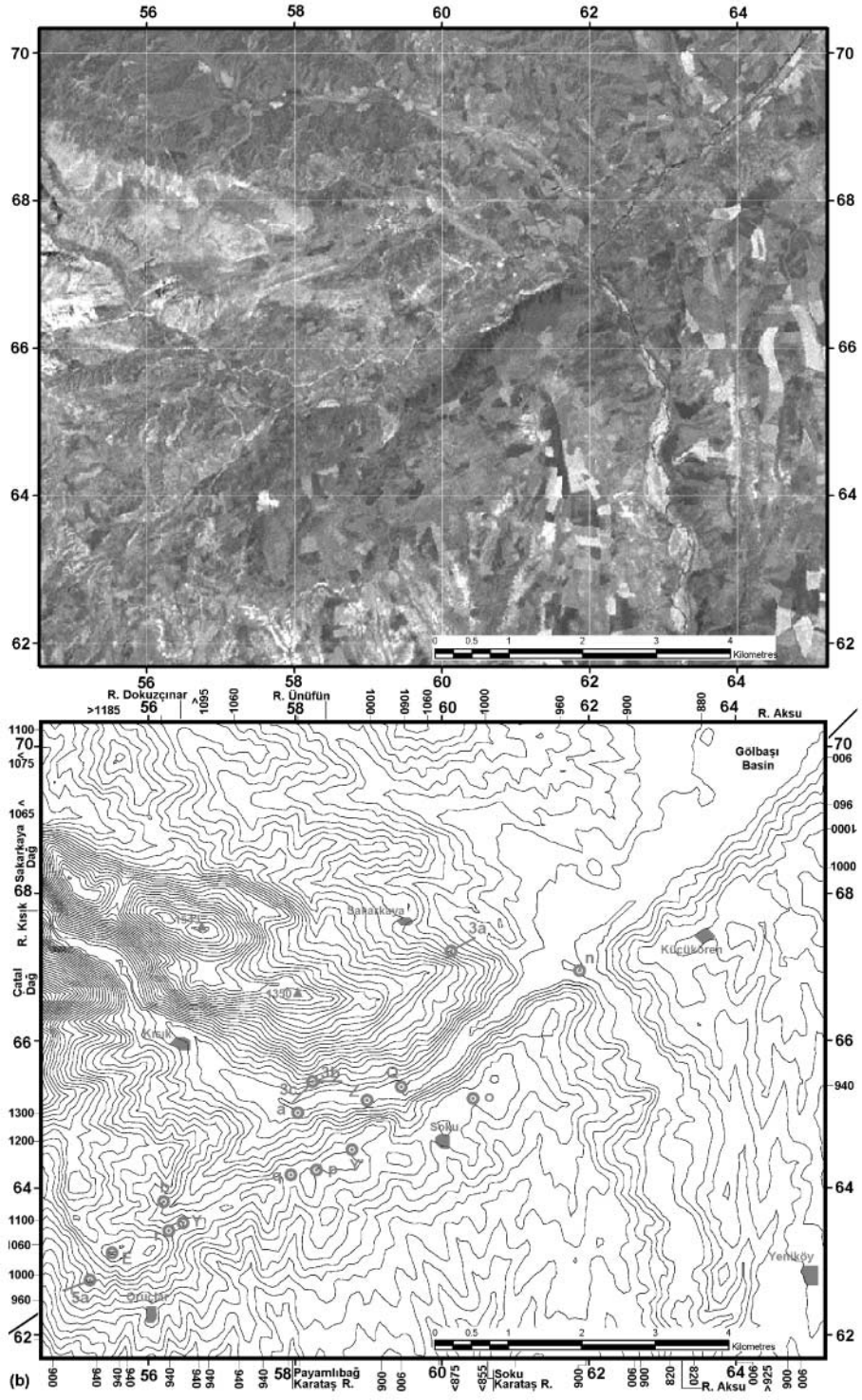

Fig. 4. Satellite image (**a**) and contour map (**b**) showing the Kısık river system. (**a**) is a Landsat ETM+ image, panchromatic band with 15 m resolution, obtained from the Global Land Cover Facility at the University of Maryland Institute for Advanced Computer Studies, College Park, Maryland (http://glcf.umiacs.umd.edu) and prepared within ERDAS Imagine. (**b**) is a contour map (contour interval 20 m) derived from Shuttle Radar Topographic Mission (SRTM) radar imagery obtained from the US Geological Survey EROS Data Center, Sioux Falls, South Dakota (http://seamless.usgs.gov), processed using Virtual Terrain Builder by VirtualTerrain.org and ERDAS Imagine and displayed using ArcGIS. This representation of the topography interpolates between measurements of a 90 m × 90 m grid of representative values of the surface altitude, determined using an interferometric radar altimeter, which operated from the space shuttle Endeavour during 11–21 February 2000 (see, e.g. JPL 1998*a*, *b*, 2005, for more details). Key localities discussed in the text, including rivers, piercing points for measuring left-lateral slip (from Tables 1 and 3), villages, photograph viewpoints and other landmarks, are labelled. The labelling of both grids is with kilometre co-ordinates within 100 × 100 km UTM quadrangle CB. Piercing points in Tables 1 and 3 have been plotted at the sites that correspond to the appropriate UTM co-ordinates of each feature. These differ from the HGK co-ordinates listed in the tables by *c*. 100–150 m north–south and *c*. 0–50 m east–west, the HGK co-ordinates being north and west of the UTM co-ordinates. This effect arises mainly because the HGK maps use a co-ordinate system that differs slightly from UTM, as previously noted (Westaway *et al*. 2004), but is also influenced, particularly in areas of high relief, by minor distortion of the surface relief that has arisen because the SRTM imaged the Earth's surface at a range of oblique angles. The nominal horizontal precision of the position of any point imaged by SRTM is ±20 m (JPL 1998*a*).

the Sincer River (Fig. 5a), passing for *c*. 1.2 km through a densely forested interfluve area, still forming the contact between ophiolite and Şelmo Formation deposits (as mapped by Tolun & Erentöz 1962; Fig. 2a) before joining the Koca River at [CB 5270 6160]. Downstream of this point, the Koca flows within a gorge in the ophiolite on the Arabian side of this fault. This river is locally at *c*. 930 m a.s.l.; in the next *c*. 3 km upstream, through Kocadere, it follows the fault, rising to *c*. 980 m a.s.l. (Fig. 6). The land surface in the ophiolite on the Arabian side is locally at a relatively uniform altitude of *c*. 1070–1090 m a.s.l. However, on the Turkish side, the landscape becomes progressively more subdued; at the downstream end of this reach the Şelmo Formation is found at up to *c*. 1100 m a.s.l. whereas at its upstream end these deposits rise just a few tens of metres above river level.

Immediately WSW of the point where the Koca River joins it, at [CB 5020 6030], the Gölbaşı–Türkoğlu Fault enters a sector of very different relief (Fig. 6), forming the contact between

Downloaded from http://jgs.lyellcollection.org/ at University of St Andrews on February 27, 2015

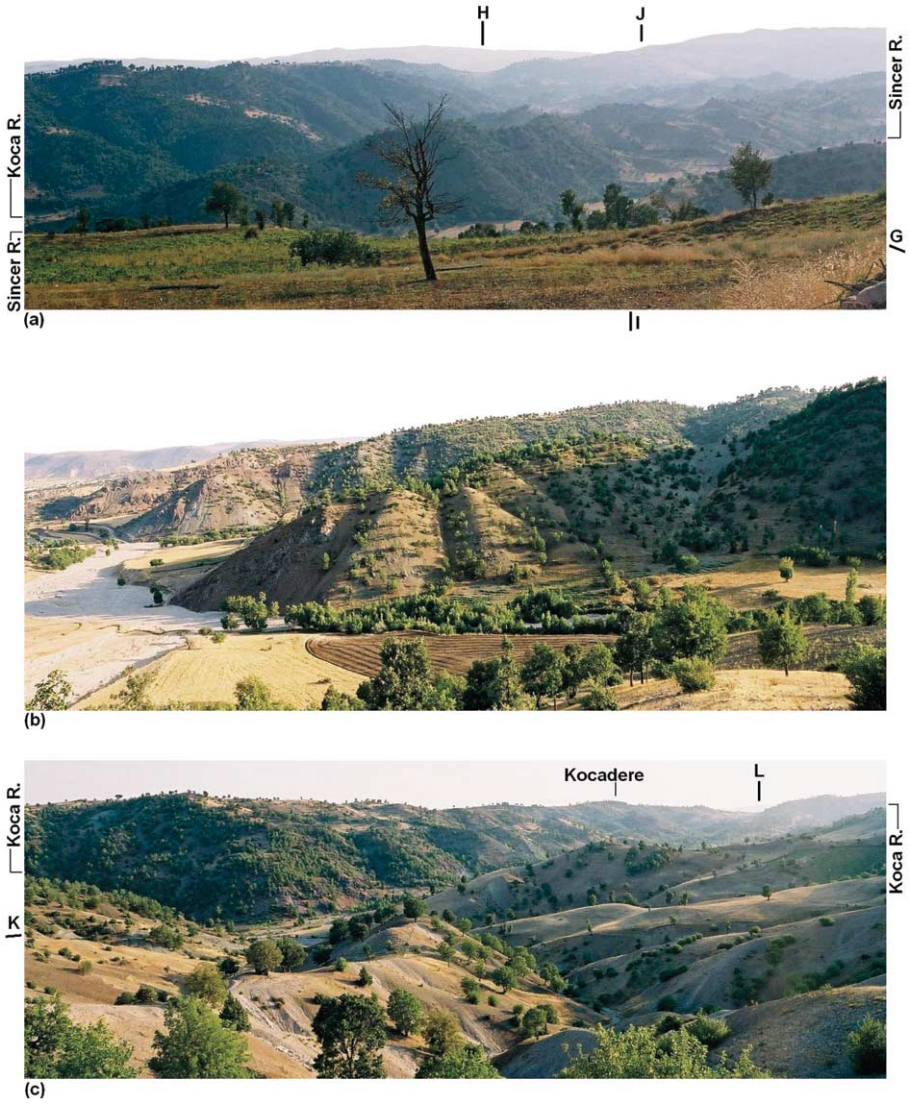

Fig. 5. (**a**) View WSW from [CB 55190 62741] SE of Karaağaç, looking at the gorges of the Koca River and its left-bank tributary, the Sincer, in the vicinity of the Gölbaşı–Türkoğlu Fault (G–H). In the distance, *c*. 6 km away (at H), the Kartaşlık col marks the boundary between the Koca and Gök river systems, beyond the offset reach of the Koca. To the right of this, the reach of the Sincer that is offset left-laterally by the Gölbaşı–Türkoğlu Fault is viewed end-on, in line with markers I–J. This fault runs through the col and along the offset reach of the Sincer river, then up a gulley to the right of the field of view. (Note the similarity in altitude of interfluve regions, with the exeption of the Midyat Group limestone to the right of the col, which stands above the typical altitude of the land surface.) (**b**) View S20°W from [CB 54261 62374], looking at the confluence of the Sincer (which flows from right to left) with its left-bank tributary, the Velikler, in the foreground and that between the Sincer and the Koca in the background. This is the eastern end of the offset reach of the Sincer, illustrated in (**a**); the ophiolite cropping out beyond the Sincer is on the Arabian side of the Gölbaşı–Türkoğlu Fault and the viewpoint on the fault line. (**c**) View S30°W from [CB 52773 62056], looking at the point where the Koca River leaves the linear valley along the Gölbaşı–Türkoğlu Fault (K–L) and passes into the ophiolite (see Tolun & Erentöz 1962). In this vicinity, folded Miocene fluvial sediment of the Şelmo Formation is present in the foreground on the Turkish side of the fault with ophiolite clearly visible on the far side of the linear valley. To the left of the field of view, the Koca River makes an abrupt bend to the right and passes into the ophiolite. In the distance, the Kartaşlık col is visible (at L), as in (a). Kocadere village (Fig. 6b) is at river level, below the point marked.

Midyat Group limestone on the Turkish side (Kardoga Tepe, rising to 1129 m a.s.l.), still with ophiolite on the Arabian side. The land surface in the ophiolite slopes gently westward from this point from *c*. 1070 m to *c*. 980 m a.s.l in *c*. 2.5 km distance, before the more deeply incised gorge system of the Gök River is reached; thus, the highest topography is now on the Turkish side of the fault. The resulting col along the fault, at *c*. 1040 m a.s.l. (north of Kartaşlık, at [CB 4980 5970]), is a distinctive landmark (Fig. 5a and c); dry valleys lead away from it both ENE towards the Koca and WSW towards the Gök (Fig. 6). Westaway & Arger (1996) deduced that this localized Kardoga Tepe–Ahlankavağı Tepe outcrop of Midyat Group limestone (their locality J, centred at [PC 4900 5960]), east of Çamlıca and Kocalar, is the truncated western end of the Kozdağ anticline near Gölbaşı, on the Arabian side of the Gölbaşı–Türkoğlu Fault (their locality M, centred at [CB 7550 7900]). The *c*. 33 km offset between these piercing points confirms the total left-lateral slip through the Gölbaşı Basin.

The Gök drainage catchment. The outlet of the Gök River from the Gölbaşı–Türkoğlu Fault (at [CB 4810 5870]), *c*. 1 km south of Kocalar, is a dramatic *c*. 120 m deep gorge, cut into ophiolite down to the *c*. 860 m a.s.l. river level (Figs 7a and 8). About 1 km farther east, truncated by the fault around [CB 4895 5905], is an unnamed dry (or underfit) valley, *c*. 40 m deep, situated between the hills Tavşan Tepe at [CB 4880 5885] and Mağara Tepe at [CB 4980 5860], which leads into the Gök *c*. 1.5 km farther downstream (Fig. 8). Two *c*. 1 km long gulleys join the fault line from the Midyat Group limestone of Ahlankavağı Tepe around [CB 4875 5955], roughly in line with this dry valley (Fig. 8), but with no surface drainage connection evident between the two. This Tavşan Tepe dry valley was evidently a former outlet for the drainage from the Turkish side of the fault, which presumably became abandoned as a result of the juxtaposition of the Kardoga Tepe–Ahlankavağı Tepe outcrop of Midyat Group limestone across it and the associated WSW offset of its former headwaters by slip on the Gölbaşı–Türkoğlu Fault.

Downloaded from http://jgs.lyellcollection.org/ at University of St Andrews on February 27, 2015

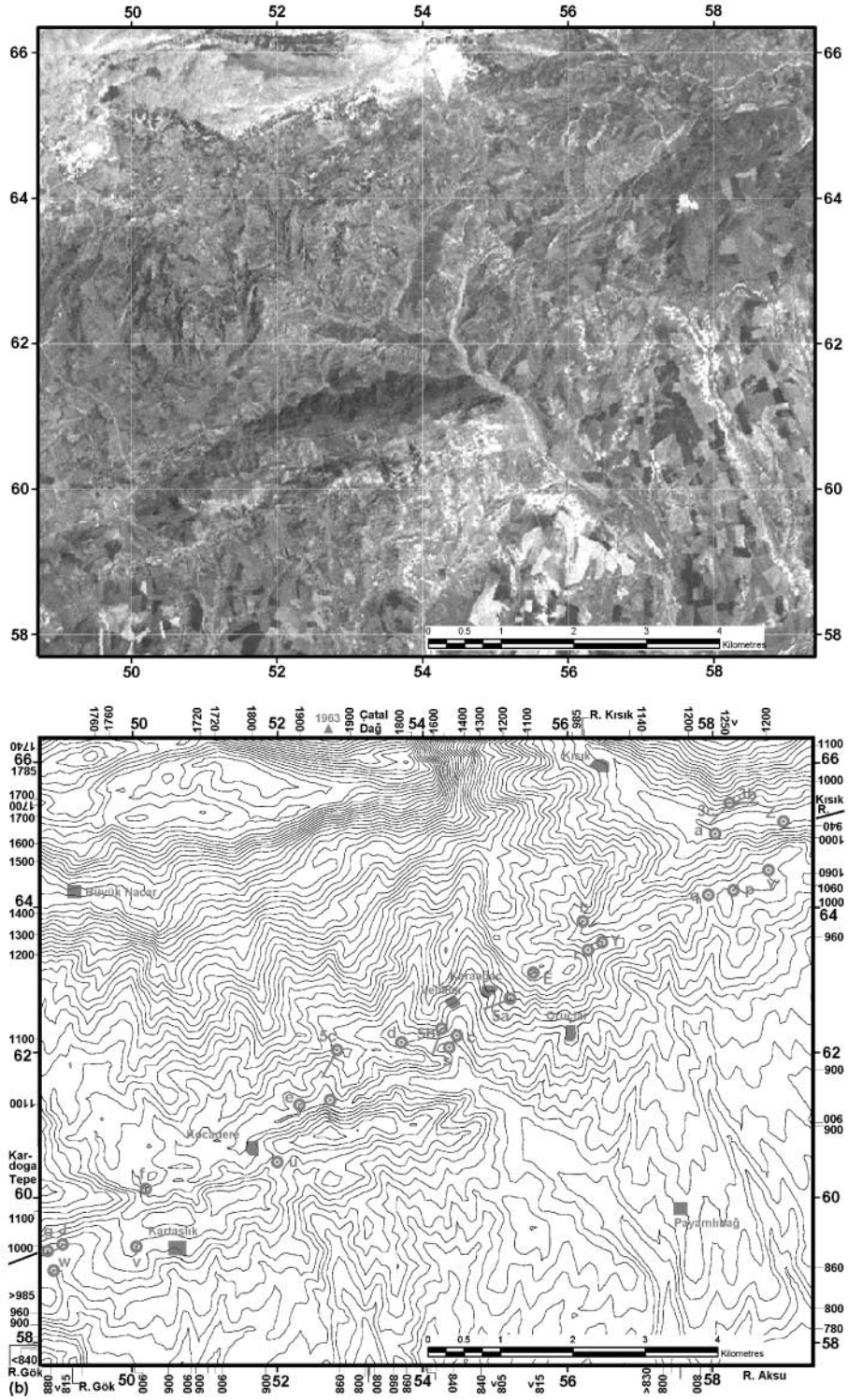

Fig. 6. Satellite image (**a**) and contour map (**b**) showing the Koca river system, obtained from the same sources and displayed in the same format as Figure 4.

For *c*. 10 km farther WSW, past Kocalar, Çamlıca and Sürülü, the Gölbaşı–Türkoğlu Fault (now oriented S57°W) is marked by the gorge of the Gök River (Fig. 8), with ophiolite on the Arabian side and, initially, clayey limestone of the Germav Formation on the Turkish side. In this sector the Gök is joined by a succession of tributaries from the Turkish side, the Mezayok, Büyük/Sıçanlı, Çatı, Çobanpınar, Karaağaç and Alanyolu rivers. The farthest upstream of these, the Alanyolu, joins the Gök headwaters at [CB 4100 5545], *c*. 8 km WSW of the modern outlet gorge. The Germav Formation is more easily erodable than the ophiolite, so, immediately upstream of the *c*. 120 m deep Gök outlet gorge the higher topography is on the Arabian side of the Gölbaşı–Türkoğlu Fault (Figs 7b and 8). However, farther WSW the land surfaces in the ophiolite and Germav Formation are both at similar levels, and the gorge depth remains a roughly uniform *c*. 120 m until the Karaağaç confluence at [CB 4225

Downloaded from http://jgs.lyellcollection.org/ at University of St Andrews on February 27, 2015

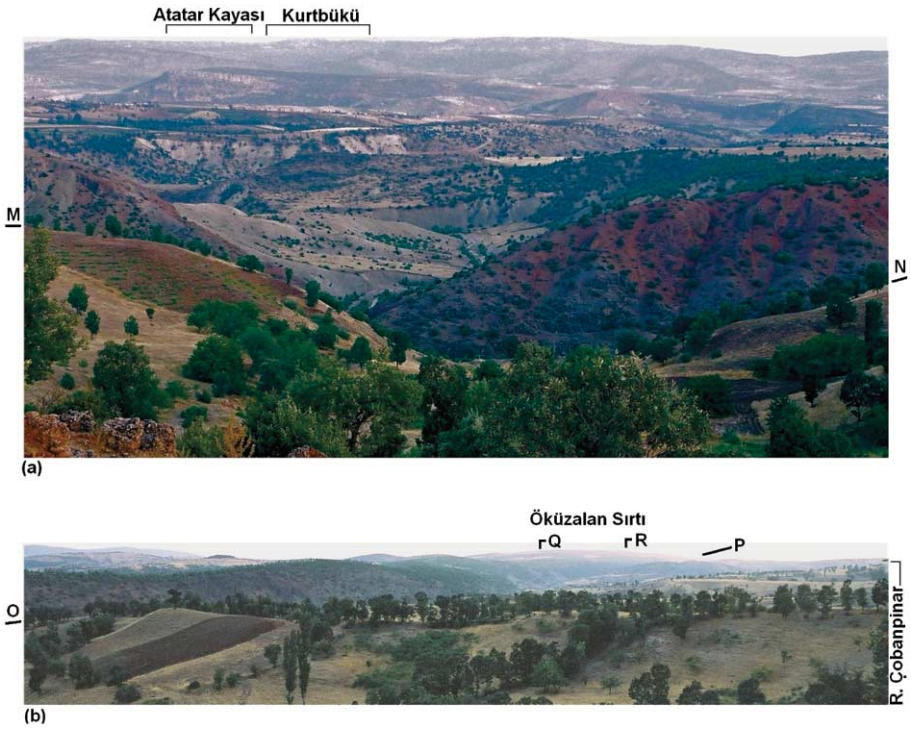

Fig. 7. (**a**) View SE from [CB 47830 58937], looking along the outlet gorge through which the Gök River leaves the Gölbaşı–Türkoğlu Fault (M–N). The view extends past Kurtbükü, across the valley of the River Aksu that is bounded by the Atatar Kayası cliff, to the skyline of the Gaziantep Plateau (Fig. 2b). (Note the transition from a narrow gorge incised into ophiolite immediately on the Arabian side of the fault to a much broader gorge, inset with low river terraces, in the unlithified marl and clayey limestone of the Germav Formation farther in the distance.) (**b**) View SW from the same place, looking along the linear valley where the Gök River is offset by the Gölbaşı–Türkoğlu Fault (O–P). The land surface adjacent to the fault on its Arabian side, in ophiolite, rises locally to a near-uniform *c*. 1000 m a.s.l. altitude, whereas the land surface on its Turkish side slopes gently towards the fault from a similar altitude to one a few tens of metres lower, then drops abruptly away to the Gök gorge about 100 m lower. For instance, the bluff in ophiolite to the right of the view in (**a**) rises to 983 m a.s.l. and the Gök river in front of it is *c*. 860–870 m a.s.l. In the distance, the land surface in the ophiolite on the Arabian side of the Gölbaşı–Türkoğlu Fault rises higher, to *c*. 1200 m a.s.l., on Öküzalan Sırtı (U in Fig. 8b). In front of this ridge, the Gök–Çobanpınar confluence (Q, equivalent to locality k in Fig. 8b) and the western limit of the ophiolite on the Turkish side of the fault (R, equivalent to X in Fig. 8b) are visible.

5605], where this river is at *c*. 1030 m a.s.l. with the surrounding land surfaces at *c*. 1150 m a.s.l. (Fig. 8). As in localities farther west on the Arabian side of the Gölbaşı–Türkoğlu Fault, the exposure in this Maastrichtian–Palaeocene sequence passes westward down-section, until ophiolite is exposed beyond the Gök gorge to the north around [CB 4165 5580]. However, the mapping by Tolun & Erentöz (1962) shows ophiolite persisting eastward within the northern flank of this gorge as far as [CB 4250 5625]. We postpone consideration of the potential value of these data as piercing points to constrain the total slip on the Gölbaşı–Türkoğlu Fault to later discussion.

The western Gölbaşı–Türkoğlu Fault. For *c*. 10 km beyond the western margin of the Gök catchment, the Gölbaşı–Türkoğlu Fault is confined within the Hatay ophiolite, with a typical local trend of S78°W (Fig. 2a). There is little fluvial incision near the fault in this sector, and no sites where significant river offsets are clearly defined, evidently as a result of the erosion resistance of the ophiolite and the limited erosional power of these headwaters. Both the fault-line valley and the surrounding landscape reach their highest altitudes in this sector (Fig. 2b), possibly because the ophiolite is locally at its thickest. The headwaters of the Gök drain ENE from [CB 3925 5440], leaving the eastern part of an expanse of linear valley floor, Göl Alanı, situated at *c*. 1250 m a.s.l., which forms the col between the Gök catchment and that of the Gökgeçit River farther WSW. In this sector, the surrounding land surface in ophiolite reaches *c*. 1310 m on the Turkish side of the fault (Gölalan Tepe; [CB 3770 5457]), with many hilltops at similar altitudes on the Arabian side, including Çatalbükü Sırtları (1292 m; [CB 4047 5400]), Gökgeçitbaşı Tepe (*c*. 1310 m; [CB 3730 5315]), and an unnamed *c*. 1300 m summit south of Göl Alanı at [CB 3845 5355].

The western end of Göl Alanı is drained WSW from [CB 3795 5395] by the Gökgeçit River, which follows the fault for *c*. 4 km to Kartal, leaving the fault line on its Arabian side at [CB 3415 5320]. Kartal village is located on the sloping surface of an alluvial fan on the Turkish side of the fault, which reaches as low as *c*. 1050 m a.s.l. in the vicinity of the Gökgeçit outlet gorge, where this river has incised to *c*. 100 m lower.

Just west of Kartal, at [CB 3405 5320], the Gölbaşı–Türkoğlu Fault crosses a low col in the alluvial fan surface, which forms the drainage divide between the Gökgeçit and Çiğli rivers. From this point, the Çiğli River follows the linear valley along the fault to Türkoğlu. Around [CB 3115 5165], *c*. 1.5 km ENE of Çiğli (or Ayanuşağı) village, the fault ceases to be confined within ophiolite on its Arabian side. For *c*. 2 km from this point it passes through an area mapped by Terlemez *et al*. (1997) as an outcrop of the 'Harabe Formation', but which seems to be more appropriately described as another large alluvial fan, shed from the ophiolite to the north, through which protrude inliers of ophiolite and Besni Formation sediment. This locality, where ophiolite ceases to be juxtaposed on

Downloaded from http://jgs.lyellcollection.org/ at University of St Andrews on February 27, 2015

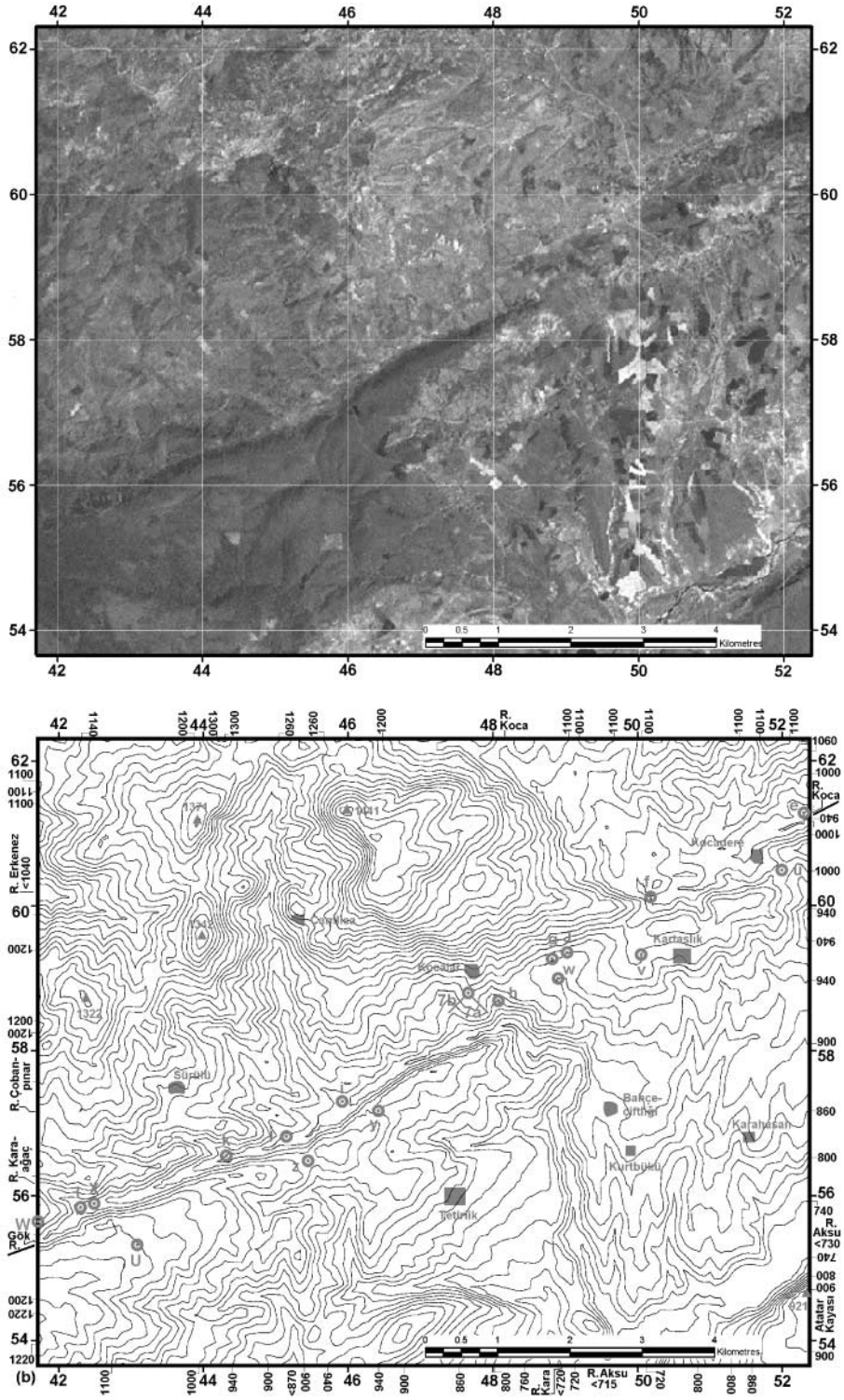

Fig. 8. Satellite image (**a**) and contour map (**b**) showing the Gök river system, obtained from the same sources and displayed in the same format as Figure 4.

the Arabian side of the fault, was used by Westaway & Arger (1996) as a piercing point (v′ in Fig. 2a) to infer 16 km of total slip, relative to the western end of the ophiolite outcrop north of the fault at Türkoğlu (v in Fig. 2a). However, as with other possible piercing points related to margins of ophiolite outcrops, the precise location of this one is difficult to establish: it could arguably be anywhere from [CB 3115 5165] (noted above) to [CB 2950 5100], representing a projection onto the fault of the westernmost outcrop of ophiolite, in the vicinity of Çiğli village.

Beyond Çiğli, the Gölbaşı–Türkoğlu Fault can be traced near the foot of the ophiolite escarpment on its Turkish side, against the Quaternary alluvial plain of the Çiğli River. At [CB 2680 5080], *c.* 3 km WSW of Çiğli, where transected by the road from Kahraman Maraş to Gaziantep, this plain is *c.* 600 m a.s.l. and the adjacent ophiolite rises to *c.* 700 m a.s.l. Moving WSW, the

Downloaded from http://jgs.lyellcollection.org/ at University of St Andrews on February 27, 2015

surface to the plain descends gradually to *c*. 470 m a.s.l. at [CB 1450 4250] near Türkoğlu, where the Aksu River crosses the fault from south to north. In contrast, the ophiolite rises to 903 m a.s.l. at the summit of Köroğlu Tepe [CB 1990 4975] before gradually descending to beneath the Quaternary alluvial plain around Türkoğlu. The Gölbaşı–Türkoğlu Fault can be clearly traced near the base of this escarpment past Tevekkelli, Kocalar and Öksüzlü, with a typical trend of S62°W, a clear fault scarp being evident for *c*. 2 km around Tevekkelli between [CB 2515 4950] and [CB 2360 4870]. Pervasive cover by Pleistocene slope deposits conceals the ophiolite west of *c*. [CB 1770 4550], near Türkoğlu. However, directly downstream of the line of this fault the Aksu at *c*. 470 m a.s.l. is flanked by bluffs rising to *c*. 540–550 m a.s.l., around [CB 1550 4450] in its right bank and as far west as [CB l300 4300] in its left bank, which may represent the westernmost part of this ophiolite unit, obscured beneath Pleistocene deposits. As with other sites already discussed, use of this margin of the ophiolite as a piercing point for estimating the total slip on the Gölbaşı–Türkoğlu Fault is thus somewhat problematical.

Analysis of Pleistocene river offsets

Figure 9a provides a schematic representation of the present-day river offsets for the Kısık, Koca and Gök systems, based as indicated on data in Figs 4, 6 and 8 and Table 1. The Kısık river system has a simple morphology, its upstream part being offset from the Kısık–Aksu outlet gorge by *c*. 4.5 km (a–n in Fig. 4b). Its only significant tributary near the Gölbaşı–Türkoğlu Fault, the Çınarcık, is offset by *c*. 2 km further and flows for this distance along the linear valley along the fault before joining the Kısık, as illustrated in Figures 4 and 6. The headwaters of the Çınarcık on the Turkish side of the fault are offset by *c*. 4.5 km from those of a tributary of the Karataş River at [CB 6040 6560], near Soku on the Arabian side (b–o in Fig. 4). Thus, restoring 4.5 km of slip on the Gölbaşı–Türkoğlu Fault juxtaposes both these headwater reaches with counterparts across the fault, the latter forming the upper reach of the now truncated Soku Karataş river.

This brief analysis can lead to the following deductions. If it is assumed that the landscape had relatively low relief in the Early Pleistocene, such that rivers were not yet entrenched into gorges, then both the Kısık and Çınarcık were able to flow across the Gölbaşı–Türkoğlu Fault with no deflection. At the start of faster regional uplift caused by climate change during MIS 22, the Kısık began to incise to try to maintain an equilibrium longitudinal profile. Being a relatively large river, with considerable erosional power at times of high seasonal flow, it was able to do this. It thus became 'locked' into its own gorge, which has since become progressively offset by left-lateral slip on the Gölbaşı–Türkoğlu Fault. In contrast, the smaller Çınarcık, with less erosional power, became deflected along the fault line to form a tributary of the Kısık, thus truncating its former lower reach on the Arabian side of the fault. We next consider whether this view, that the Gölbaşı–Türkoğlu Fault has slipped by *c*. 4.5 km since MIS 22, is supported by the evidence from the Koca and Gök river systems.

For the Koca system, Figure 9b indicates that, after 4.5 km of left-lateral slip is restored, the points where the Sincer and Velikler rivers reach the fault line on its Turkish side are juxtaposed opposite what are now truncated headwaters of affluents of the Soku Karataş River and of another Karataş River, which flows separately into the Aksu past the village of Payamlıbağ (c–p and d–q in Fig. 6b). The Kaykırtlı tributary of the Koca is aligned opposite the truncated headwaters of a more

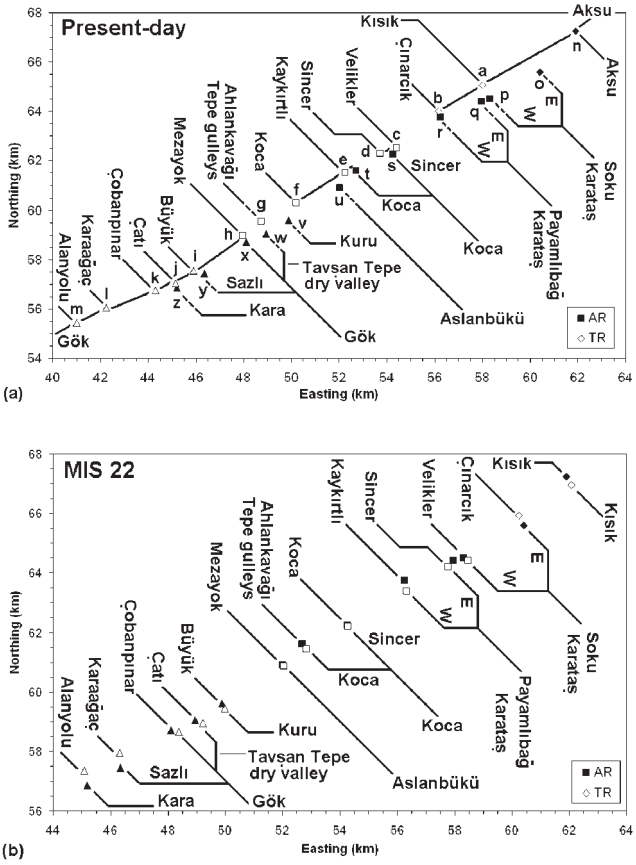

Fig. 9. (**a**) Present-day pattern of river offsets along the studied part of the Gölbaşı–Türkoğlu Fault, labelled to indicate piercing points listed in Table 1 and to schematically represent the associated river geometry. Dashed lines indicate rivers that are at present truncated at the Gölbaşı–Türkoğlu Fault. (**b**) Inferred river pattern after restoration of 4.5 km of left-lateral slip directed towards S65°W, in a reference frame fixed to the Arabian plate, with inferred schematic contemporaneous geometries of river courses. (See text for discussion.)

westerly affluent of the Payamlıbağ Karataş River (e–r in Fig. 6b), which is now a right-bank tributary of the Koca, joining it downstream of the fault. The Koca itself aligns with the point, illustrated in Figure 9b, where the combined Sincer and Velikler now leave the fault line on its Arabian side (f–s in Fig. 4b).

These correlations imply that a complex sequence of drainage diversions affected what are now tributaries of the Koca system during the Mid–Late Pleistocene. For instance, the modern outlet gorge of the Koca away from the fault line is predicted to have aligned in MIS 22 with the gulleys (noted above; g in Fig. 6b) in the karstified outcrop of Midyat Group limestone on the Turkish side of the fault forming Ahlankavağı Tepe near Kocalar. The modern offset of the Koca, upstream of this present outlet, from [CB 5020 6030] to [CB 5270 6160] (f–t in Fig. 6b) is *c*. 2.8 km, suggesting that it adopted this route around 870 ka × 2.8/4.5 or *c*. 540 ka, indicating MIS 14. It had presumably maintained its course through its original outlet until that time, before its upper reaches were captured by its present outlet gorge, which appears to have been the original drainage outlet for the Ahlankavağı Tepe area. The Velikler, Sincer and Kaykırtlı were presumably diverted into the linear valley along the Gölbaşı–Türkoğlu Fault immediately after the increase in

Downloaded from http://jgs.lyellcollection.org/ at University of St Andrews on February 27, 2015

Table 1. *Candidate piercing points for the slip on the Gölbaşı–Türkoğlu Fault from river offsets*

Code	Block	UTM co-ordinates	Description
Inlets into the line of the Gölbaşı–Türkoğlu Fault			
a	TR	CB 5800 6505	Kısık enters linear valley of GTF, north of Soku
b	TR	CB 5615 6402	Çınarcık tributary of Kısık enters linear valley of GTF, NE of Karaağaç
c	TR	CB 5440 6250	Velikler tributary of Sincer enters linear valley of GTF, south of Karaağaç
d	TR	CB 5370 6230	Sincer enters linear valley of GTF, SW of Karaağaç
e	TR	CB 5225 6150	Kaykırtlı tributary of Koca enters linear valley of GTF, ENE of Kocadere
f	TR	CB 5020 6030	Koca enters linear valley of GTF, WSW of Kocadere
g	TR	CB 4875 5955	Gulleys draining from limestone area of Ahlankavağı Tepe join GTF
h	TR	CB 4797 5897	Mezayok tributary of Gök enters linear valley of GTF, SE of Kocalar
i	TR	CB 4590 5755	Büyük tributary of Gök enters linear valley of GTF, SW of Kocalar
j	TR	CB 4515 5705	Çati tributary of Gök enters linear valley of GTF, SE of Sürülü
k	TR	CB 4430 5675	Çobanpınar tributary of Gök enters linear valley of GTF, south of Sürülü
l	TR	CB 4225 5605	Karaağaç tributary of Gök enters linear valley of GTF, SW of Sürülü
m	TR	CB 4100 5545	Alanyolu tributary of Gök enters linear valley of GTF, SW of Sürülü
Outlets from the line of the Gölbaşı–Türkoğlu Fault			
n	AR	CB 6190 6725	Kısık joins Aksu and combined river exits linear valley of GTF, west of Küçükören
o	AR	CB 6040 6560	Truncated headwaters of east branch of Soku Karataş river, east of Soku
p	AR	CB 5830 6450	Truncated headwaters of west branch of Soku Karataş river, NE of Oruçlar
q	AR	CB 5795 6440	Truncated headwaters of east branch of Payamlıbağ Karataş river, NE of Oruçlar
r	AR	CB 5625 6375	Truncated headwaters of west branch of Payamlıbağ Karataş river, NE of Oruçlar
s	AR	CB 5425 6225	Velikler joins Sincer and combined river exits linear valley of GTF, south of Karaağaç
t	AR	CB 5270 6160	Koca exits linear valley of GTF, ENE of Kocadere
u	AR	CB 5200 6090	Truncated headwaters of Aslanbükü river, south of Kocadere
v	AR	CB 4990 5960	Truncated headwaters of Kuru river, west of Kartaşlık
w	AR	CB 4895 5905	Dry valley between Tavşan Tepe and Mağara Tepe
x	AR	CB 4810 5870	Gök river exits linear valley of GTF, south of Kocalar
y	AR	CB 4635 5745	Truncated headwaters of Sazlı river, SW of Kocalar
z	AR	CB 4520 5685	Truncated headwaters of Kara river, SE of Sürülü

Co-ordinates listed in this table have been measured from Harita Genel Komutanlığı (HGK) 1:25 000 scale topographic maps. GTF, Gölbaşı–Türkoğlu Fault

regional uplift rates, their outlet from then on having been the gorge that continues to be occupied by the Sincer, upstream of its modern confluence with the Koca on the Arabian side of the fault. For much of the Mid-Pleistocene, these rivers would thus have been offset to the right across this linear valley, this pattern of offsets having since been gradually cancelled out by the progressive left-lateral slip on the fault.

For what is now the Gök system, restoring 4.5 km of left-lateral slip aligns each of the modern left-bank tributaries of the Gök, from the Turkish side of the Gölbaşı–Türkoğlu Fault, with an initial counterpart on the Arabian side. Thus, the Ahlankavağı Tepe gulleys align with the modern outlet gorge of the Koca (g–t in Fig. 6b), the Mezayok aligns with the Aslanbükü (h–u in Fig. 8b), the Büyük with the Kuru (i–v), the Çatı with the Tavşan Tepe dry valley (j–w), the Çobanpınar with the modern outlet gorge of the Gök (k–x), the Karaağaç with the Sazlı (l–y), and the Alanyolu with the Kara (m–z; Figs 8b and 9b). It thus appears that the Çobanpınar has maintained its original geometry, with progressive deflection to the left as a result of slip on the Gölbaşı–Türkoğlu Fault; the Alanyolu and Karaağaç appear to have been promptly captured by and deflected into this system following the increase in regional uplift rates. In contrast, the substantial incision evident in what is now the Tavşan Tepe dry valley suggests that, for a time, it formed the outlet for the Büyük and/or the Çatı. However, such a geometry can have been maintained until no later than *c.* 600 ka (MIS 15), by which time the Büyük is predicted to have become juxtaposed opposite the modern Gök outlet gorge. This restoration suggests that the Mezayok, which is now a tributary of the Gök, was, for a time after MIS 22, a tributary of the Koca, joining it at the outlet from what is now the dry valley ENE of the Kartaşlık col. The *c.* 0.5 km length of this dry valley suggests that it was occupied by the Mezayok for around 100 ka, before this river was captured by the Gök system.

The consistency of these *c.* 4.5 km river offsets suggests strongly that the stated hypothesis is tenable. Figure 9b indicates that the overall fit of the drainage restoration would be significantly degraded if the slip were adjusted by more than ±0.1 km. The 13 individual measurements of offsets between piercing points listed in Table 2 give a mean value of 4.44 ± 0.06 km (±2σ). The left-lateral slip rate on the Gölbaşı–Türkoğlu Fault, time-averaged since MIS 22 (870 ka), is thus estimated as 5.10 ± 0.07 mm a^{-1}.

Discussion

As already noted, the Westaway (2004*a*) kinematic model predicts Turkish–Arabian relative motion at 8.0 mm a^{-1} towards S48°W in the vicinity of Gölbaşı. The above estimate that 5.1 mm a^{-1} of this motion occurs on the Gölbaşı–Türkoğlu Fault leaves an additional 2.9 mm a^{-1} unaccounted for, which can be presumed to be partitioned between the Sürgü Fault (Fig. 1) and the array of NNE–SSW-striking faults south of the Gölbaşı–Türkoğlu (Fig. 2). The combined total slip on the Gölbaşı–Türkoğlu Fault and these NNE–SSW-striking faults was estimated as 33 km by Westaway & Arger (1996), from offsets J–M and Q–T in Figure 2a, a deduction that is supported by the present study. To make any further refinement of the regional kinematics, an independent estimate of the total slip on the Gölbaşı–Türkoğlu Fault is needed. Earlier discussion established that, because the precise locations of the piercing points that were used (after Tolun & Erentöz 1962) cannot be unambiguously established, the reasoning that led to the Westaway & Arger (1996) estimate of 16 km needs to be re-examined. As Westaway & Arger (1996) noted, the

Downloaded from http://jgs.lyellcollection.org/ at University of St Andrews on February 27, 2015

Table 2. *Offsets between piercing points from river gorges*

Piercing points	Separation	
	Distance (km)	Azimuth
an	4.48	S61°W
bo	4.53	S70°W
cp	4.38	S63°W
dq	4.39	S75°W
er	4.59	S61°W
fs	4.49	S64°W
gt	4.45	S63°W
hu	4.47	S64°W
iv	4.59	S61°W
jw	4.29	S62°W
kx	4.27	S63°W
ly	4.33	S71°W
mz	4.43	S72°W

See Table 1 for descriptions and co-ordinates of these piercing points; see Figures 4, 6 and 8 for their locations.

Ahlankavağı Tepe–Kozdağ piercing point (J–M in Fig. 2a) adjoined the site where, at its time of formation, the Gölbaşı–Türkoğlu Fault splayed from the zone of NNE–SSW-striking left-lateral faulting farther south. To constrain the slip on just the Gölbaşı–Türkoğlu Fault one must thus investigate sites to the west of these points.

The possibility of differential erosion between different parts of any strike-slip fault in SE Turkey (see Westaway & Arger 1996) makes it difficult to establish exact matches between piercing points, and also means that apparent offsets between outcrop boundaries do not necessarily equal their true strike-slip offset. However, four general forms of evidence can provide piercing points to constrain the total slip on the Gölbaşı–Türkoğlu Fault: the unconformities between the ophiolite and overlying sediments at the eastern margin of the ophiolite; the relief at the western margin of the ophiolite; the highest summits within the ophiolite; and the locations of the highest ridges within the ophiolite. Table 3 lists potential candidate piercing points, and Table 4 lists the distances by which pairs of these that might be thought *a priori* to correlate are offset. The preponderance of evidence suggests *c*. 19 km of offset, indicating the total slip on the Gölbaşı–Türkoğlu Fault. The most reliable geomorphological indicator seems to be the match between the ridge of ophiolite forming Köroğlu Tepe on the Turkish side of the Gölbaşı–Türkoğlu Fault NE of Türkoğlu against the highest topography on the Arabian side of the Gölbaşı–Türkoğlu Fault south of Göl Alanı (offsets R–V and S–U in Table 4). Matching of the highest topography on the Turkish side of the Gölbaşı–Türkoğlu Fault north of Göl Alanı against that on the Arabian side around Karaağaç Tepe (offset B–E in Table 4) provides a similar estimate, as does matching the westernmost evidence of the presence of ophiolite near Türkoğlu on the Turkish side of the Gölbaşı–Türkoğlu Fault and near Çiğli on the Arabian side (H–L in Table 4). Matching the contact between ophiolite and Besni Formation in the Gök gorge near Sürülü on the Turkish side of the Gölbaşı–Türkoğlu Fault against its counterpart in the Kısık gorge on the Arabian side near Soku gives a similar estimate (X–Z in Table 4). Matching the eastern margins of the ophiolite outside these gorges (W–Y in Table 4) underestimates the other values by *c*. 1 km. A possible cause of this mismatch is faster erosion of the feather edge of the Besni Formation adjacent to the Gök gorge, possibly as a result of higher rainfall in this higher-altitude locality; if the Besni Formation persisted farther west in this locality the offset measurement would be greater. Alternatively, the ophiolite may persist farther east on the Arabian side of the Gölbaşı–Türkoğlu Fault, leading to the alternative *c*. 19 km slip estimate W–Y′ in Table 4.

Dividing this 19 km estimate for the total slip on the Gölbaşı–Türkoğlu Fault into the 5.10 ± 0.07 mm a^{-1} slip rate deduced earlier gives an estimated age (assuming that the same slip rate has been maintained throughout) for the Gölbaşı–Türkoğlu Fault of 3.73 ± 0.05 Ma. Conversely, dividing the total of 33 km of slip across all left-lateral fault strands in the Gölbaşı area by the 8.0 mm a^{-1} rate of Turkish–Arabian relative motion (from Westaway 2004*a*) gives a higher age estimate, of 4.13 Ma, and implies that 14 km of this 33 km of relative motion was taken up on NNE–SSW-striking faults south of Gölbaşı. A possible explanation for this discrepancy, after Westaway (2004*a*), is that part of the slip on these NNE–SSW-striking faults predates the modern East Anatolian Fault Zone system (for instance, it may have linked into its predecessor farther NE, the Malatya–Ovacık Fault Zone; see Westaway & Arger 2001). The total of Turkish–Arabian relative motion expected since 3.73 ± 0.05 Ma can be estimated as 3.73 ± 0.05 Ma $\times$ 8.0 mm a^{-1} or 29.8 ± 0.4 km. Neglecting for the time being, for convenience of calculation, any slip on the Sürgü Fault on this time scale, one can infer that a minimum of *c*. 11 km of the slip on these NNE–SSW-striking faults has accompanied the modern geometry of the East Anatolian Fault Zone; the rest (up to *c*. 3 km) may thus predate it. Alternatively, the 8.0 mm a^{-1} rate of Turkish–Arabian relative motion at Gölbaşı, from Westaway (2004*a*), which has formed the basis for these calculations (and which was derived from GPS data, from McClusky *et al*. (2000), not geological evidence) may slightly underestimate the overall time-averaged rate. Adjusting this rate upward to 8.85 ± 0.12 mm a^{-1} would predict 33 km of total slip since 3.73 ± 0.05 Ma, thus accounting for the geological evidence from this area, without any need for any of this slip to predate the Mid-Pliocene initiation of the East Anatolian Fault Zone system. More detailed analysis of this issue will require quantitative analysis of the array of NNE–SSW-striking faults south of Gölbaşı, and so is beyond the scope of the present study. However, adding the *c*. 4 km estimate of left-lateral slip on the Sürgü Fault (Westaway 2004*a*) to the *c*. 33 km on the Gölbaşı–Türkoğlu Fault gives *c*. 37 km, suggesting an overall local rate of Turkish–Arabian relative motion of 9.92 ± 0.13 mm a^{-1} since 3.73 ± 0.05 Ma. Assuming the same position for the pole of rotation as was deduced by Westaway (2004*a*) (Fig. 1), the Turkish–Arabian Euler vector adjusts to $0.89 \pm 0.01°$ Ma^{-1} about 33.4°N, 42.3°E.

It now appears that increases in uplift rates following the onset of 100 ka Milankovitch climate cyclicity in the late Early Pleistocene (MIS 22) are a widespread phenomenon worldwide, which can be attributed to coupling between surface processes and the lower-crustal flow that is induced in response in order to maintain isostatic equilibrium (e.g. Westaway 2001, 2002*b*, *c*). The analysis in the present sudy indicates that the onset of this combination of coupled processes led to a complex series of drainage adjustments in the study region, as rivers became progressively entrenched into what had previously been a low-relief landscape with linear drainage. However, this sequence of adjustments seems to have been completed in this study region no later than MIS 14, since when the new, much more dendritic, drainage geometry that developed has remained stable. As previously inferred (e.g. Arger *et al*. 2000; Demir *et al*. 2004, 2005), this uplift has nothing directly to do with the left-lateral

Downloaded from http://jgs.lyellcollection.org/ at University of St Andrews on February 27, 2015

Table 3. *Candidate piercing points for the total slip on the Gölbaşı–Türkoğlu Fault*

Code	Block	UTM co-ordinates	Description
Western margin of ophiolite			
H	TR	CB 1300 4300	Western end of bench *c*. 540 m a.s.l. above Aksu river left bank north of Türkoğlu
K	TR	CB 1550 4450	Bench *c*. 550 m a.s.l. above Aksu river right bank north of Türkoğlu
L	AR	CB 2950 5100	Projection of westernmost ophiolite outcrop to fault west of Çiğli, *c*. 700 m a.s.l.
N	AR	CB 3115 5165	Western limit of ophiolite enclosing linear valley east of Çiğli, *c*. 900 m a.s.l.
Eastern margin of ophiolite			
W	TR	CB 4165 5580	Most easterly point with ophiolite outcrop north of Gök gorge near Sürülü
X	TR	CB 4250 5615	Most easterly point with ophiolite beneath Besni Fm in Gök gorge
Y	AR	CB 5640 6375	Most easterly point with ophiolite outcrop south of Kısık gorge near Soku
Y′	AR	CB 5875 6475	Most easterly point with ophiolite outcrop south of Kısık gorge near Soku
Z	AR	CB 5900 6550	Most easterly point with ophiolite beneath Besni Fm in Kısık gorge near Soku
Highest summits in ophiolite			
A	TR	CB 2020 4760	Projection of Köroğlu Tepe summit, 903 m [CB 1990 4975], to fault
B	TR	CB 3770 5457	Summit of Gölalan Tepe, *c*. 1310 m
C	AR	CB 3730 5315	Summit of Gökgeçitbaşı Tepe, *c*. 1310 m
G	AR	CB 3845 5355	Unnamed *c*. 1300 m summit south of Göl Alanı
D	AR	CB 4047 5400	Highest point on Çatalbükü Sırtları, 1292 m
E	AR	CB 5550 6332	Summit of Karaağaç Tepe, 1249 m
Length of highest ridge in ophiolite			
R	TR	CB 1675 4675	700 m contour at west end of ridge NW of Öksüzlü
S	TR	CB 2490 5005	700 m contour at east end of ridge, east of Beyazhöyük Tepe, north of Tevekkeli
V	AR	CB 3468 5295	1150 m contour at west end of ridge, Çetinyolu Sırtı, SE of Kartal
U	AR	CB 4305 5548	1150 m contour at east end of ridge, Öküzalan Sırtı, SW of Sürülü

Co-ordinates listed in this table have been measured from Harita Genel Komutanlığı 1:25 000 scale topographic maps. Piercing point Y is derived from the mapping by Tolun & Erentöz (1962). Y′ is derived from our own observations of the eastern limit of high and rough topography that is characterizes other ophiolite outcrop in this region (see the main text, also Fig. 3c and its caption).

Table 4. *Offsets between piercing points for total slip*

Piercing points	Separation	
	Distance (km)	Azimuth
Western margin of ophiolite		
HL	18.34	S64°W
KN	17.21	S65°W
Eastern margin of ophiolite		
WY	16.76	S62°W
WY′	19.30	S62°W
XZ	18.97	S61°W
Highest summits in ophiolite		
AC	17.41	S71°W
AD	21.26	S72°W
AG	19.20	S72°W
BE	19.83	S64°W
Length of highest ridge in ophiolite		
RV	18.97	S71°W
SU	18.94	S71°W

See Table 3 for descriptions and co-ordinates of these piercing points; see Figures 4, 6 and 8 for their locations.

faulting, and would be occurring even if this region were not within a plate boundary zone.

Regarding rates and amounts of uplift during the Mid- to Late Pleistocene, it is evident that, with minor exceptions, river gorges that have been incised on this time scale are *c*. 100–120 m deep. This includes the gorge of the Aksu trunk channel throughout most of its length, and many of its tributary gorges (see above, also Figs 4, 6 and 8). The principal exception is in the headwaters of tributary gorges, where they have little erosional power and so have been unable to incise at the same pace as the regional uplift, as is also widely observed in many other regions. Restoring this incision indicates that this study region had much lower relief in the Early Pleistocene than at present. The principal relief that already existed related to the earlier folding of the erosion-resistant Midyat Group limestone, notably as mountains such as Sakarkaya Dağ and Çatal Dağ (Fig. 4), as well as in smaller folded inliers of it such as Atatar Kayası (Fig. 7a). Other relief dating from this time related to the roughness of the land surface in the ophiolite. In some places the ophiolite has effectively 'armoured' the flanks of adjoining deposits that would otherwise have been more easily erodable, thus protecting them from erosion, for instance preserving extensive deposits of the Besni and Germav Formations in much of the Gök system on the Turkish side of the Gölbaşı–Türkoğlu Fault (Fig. 8). However, elsewhere, where no such 'armouring' effect has been possible, the more easily erodable deposits have largely been removed from the region, a notable example being provided by the Koca river west of Kocadere (Fig. 6) which appears to have removed the deposits of the Şelmo Formation from the northern flank of its gorge almost as fast as it has itself incised, creating a low-relief landscape just above modern river level.

As already noted, the largest river in the Arabian Platform of SE Turkey, the Euphrates (Fırat) has a well-developed staircase of Pleistocene terraces, notably around Birecik (e.g. Minzoni-Deroche & Sanlaville 1988; Fig. 2b). As illustrated in Figure 2b, this river flows *c*. 50–60 km east of the present study region; it is thus expected to indicate the same uplift history as the smaller rivers investigated in the present study. The terrace that is now thought (Demir *et al*. 2004, 2005) to date from MIS 22 is found *c*. 110 m above present river level, indicating essentially the same amount of incision on this time scale as is observed in the river systems investigated in the present study, even though the latter are much smaller. We thus interpret this incision as a good proxy

Downloaded from http://jgs.lyellcollection.org/ at University of St Andrews on February 27, 2015

for regional uplift by a near-uniform distance across this region on this time scale.

The principal evidence for lateral variations in regional uplift in the present study region is provided by the difference in altitude, by *c*. 400–500 m, between the outcrops north of the Gölbaşı–Türkoğlu Fault near Türkoğlu and south of the Gölbaşı–Türkoğlu Fault in the vicinity of Göl Alanı (Table 3). We presume that this differential effect is the net isostatic result, since the Pliocene, of the sediment loading that has occurred in the Plio-Pleistocene depocentres that adjoin the Gölbaşı–Türkoğlu Fault around Türkoğlu and Kahraman Maraş (Fig. 2a). However, detailed calculation of this effect, for instance using the physics-based modelling approach of Westaway (2002*a*; Westaway *et al*. 2004), is beyond the scope of this study.

It is becoming increasingly clear that increases in uplift rates, revealed by fluvial incision, resulting from global climate change in the late Early Pleistocene, are widely observed, being well-documented in temperate latitudes (e.g. Westaway 2001, 2002*b*, *c*) and also evident within the tropics (Bridgland & Westaway 2005*a*, *b*), not just in Europe where this effect was first identified (by Kukla 1975, 1978). It follows that detailed analysis of the fluvial geomorphology along many other active strike-slip faults worldwide may well provide analogous datasets to that developed in the present study, which can give the slip rate time-averaged since MIS 22. Such estimates are likely to be extremely useful, for instance in earthquake hazard assessment, for testing regional kinematic models, and for comparison with shorter time scale datasets from trenching and GPS. The basis of a powerful new method is thus apparent.

Conclusions

In the Arabian Platform of SE Turkey, fluvial incision since the late Early Pleistocene has accompanied regional surface uplift, as the isostatic response to regional erosion. This incision, typically by *c*. 110 ± 10 m, starting in or around MIS 22 at 870 ka, has progressively 'locked' rivers into their gorges in landscape that formerly had much lower relief. We use this effect to estimate 4.44 ± 0.06 km of left-lateral slip on this time scale on the Gölbaşı–Türkoğlu Fault from offset river gorges, giving a slip rate of 5.10 ± 0.07 mm a^{-1}. Piercing points indicate that this fault has slipped a total of 19 km, making its age 3.73 ± 0.05 Ma. A total of 33 km of relative motion between the Turkish and Arabian plates is documented on this time scale in the vicinity of Gölbaşı, at an overall time-averaged rate of 8.85 ± 0.12 mm a^{-1}. This analysis indicates the basis for a new method for estimating slip rates, time-averaged since the late Early Pleistocene, which is potentially applicable to strike-slip fault zones worldwide.

This study contributes to IGCP 449 'Global Correlation of Late Cenozoic Fluvial Deposits' and to IGCP 518 'Fluvial sequences as evidence for landscape and climatic evolution in the Late Cenozoic'.

References

Adiyaman, Ö. & Chorowicz, J. 2002. Late Cenozoic tectonics and volcanism in the northwestern corner of the Arabian Plate; a consequence of the strike-slip Dead Sea Fault Zone and the lateral escape of Anatolia. *Journal of Volcanology and Geothermal Research*, **117**, 327–345.

Al-Riyami, K., Robertson, A.H.F., Dixon, J. & Xenophontos, C. 2002. Origin and emplacement of the Late Cretaceous Baer-Bassit Ophiolite and its metamorphic sole in NW Syria. *Lithos*, **65**, 225–260.

Arger, J., Mitchell, J. & Westaway, R. 2000. Neogene and Quaternary volcanism of south-eastern Turkey. *In:* Bozkurt, E., Winchester, J.A. & Piper, J.D.A. (eds) *Tectonics and Magmatism of Turkey and the Surrounding Area*. Geological Society, London, Special Publications, **173**, 459–487.

Arpat, E. & Şaroğlu, F. 1972. Doğu Anadolu Fayı ile ilgili bazı gözlem ve düşünceler. *MTA Bülteni*, **73**, 1–9.

Besançon, J. & Geyer, B. 2003. La géomorphologie de la basse vallée de l'Euphrate Syrien: contribution à l'étude des changements de l'environnement géographique au Quaternaire. *In:* Geyer, B. & Montchambert, J.-Y. (eds) *La Basse Vallée de l'Euphrate Syrien du Néolithique à l'Avenement de l'Islam. Vol. 1: Text. Mission Archéologique de Mari, Vol. 6*. Institut Français du Proche Orient, Beirut, 7–59.

Besançon, J. & Sanlaville, P. 1981. Aperçu géomorphologique sur la vallée de l'Euphrate Syrien. *Paléorient*, **7**(2), 5–18.

Bridgland, D.R. & Westaway, R. 2005a. Late Cenozoic landscape evolution as evidenced from the fluvial record: a review of data and results from IGCP 449. *Global and Planetary Change*, in press.

Bridgland, D.R. & Westaway, R. 2005b. Preservation patterns of Late Cenozoic fluvial deposits and their implications: results from IGCP 449. *Quaternary International*, in press.

Bridgland, D., Philip, G., Westaway, R. & White, M. 2003. A long Quaternary terrace sequence in the valley of the River Orontes, near Homs, Syria. *Current Science*, **84**, 1080–1089.

Chorowicz, J., Luxey, P., Lyberis, N., Carvalho, J., Parrot, J.F., Yürür, T. & Gündoğdu, M.N. 1994. The Maraş triple junction (southern Turkey) based on digital elevation model and satellite imagery interpretation. *Journal of Geophysical Research*, **99**, 20225–20242.

Collier, R.E.L., Leeder, M.R., Trout, M., Ferentinos, G., Lyberis, E. & Papatheodorou, G. 2000. High sediment yields and cool, wet winters: test of last glacial paleoclimates in the northern Mediterranean. *Geology*, **28**, 999–1002.

Delaloye, M. & Wagner, J.-J. 1984. Ophiolites and volcanic activity near the western edge of the Arabian Plate. *In:* Dixon, J.E. & Robertson, A.H.F. (eds) *The Geological Evolution of the Eastern Mediterranean*. Geological Society, London, Special Publications, **17**, 225–233.

Delaloye, M., Vuagnat, M. & Wagner, J.-J. 1977. K–Ar ages from the Kizil Dagh ophiolitic complex (Hatay, Turkey) and their interpretation. *In:* Biju-Duval, B. & Montadert, L. (eds) *Structural History of the Mediterranean Basins*. Technip, Paris, 73–78.

Demir, T., Yeşilnacar, & Westaway, R. 2004. River terrace sequences in Turkey: sources of evidence for lateral variations in regional uplift. *Proceedings of the Geologists' Association*, **115**, 289–311.

Demir, T., Westaway, R., Bridgland, D.R., Seyrek, A. & Beck, A. 2005. Terrace staircases of the River Euphrates in southeast Turkey, northern Syria and western Iraq: evidence for regional surface uplift. *Quaternary Science Reviews*, in press.

Derman, A.S. 1999. Braided river deposits related to progressive Miocene surface uplift in Kahraman Maraş area, SE Turkey. *Geological Journal*, **34**, 159–174.

Erol, O., Akkan, E., Elibüyük, M. & Doğu, A.F. 1979. The present and Quaternary natural environmental conditions in the lower Euphrates region. *In: Middle East Technical University Lower Euphrates Project Publications, Series I, No. 3, Lower Euphrates Project, 1978–1979 Activities*. Türk Tarih Kurumu Basimevi, Ankara, 15–27.

JPL 1998a. Shuttle Radar Topographic Mission: mapping the world in three dimensions. Jet Propulsion Laboratory Report 400-713 7/98. Available online: http://www2.jpl.nasa.gov/srtm/factsheet_tech.pdf

JPL 1998b. Seeing Earth's surface in 3-D: Shuttle Radar Topographic Mission. Jet Propulsion Laboratory Report 400-714 7/98. Available online: http://www2.jpl.nasa.gov/srtm/factsheet_pub.pdf

JPL 2005. Shuttle Radar Topographic Mission: the mission to map the world. Jet Propulsion Laboratory, California Institute of Technology, Pasadena, CA. Available online: http://www2.jpl.nasa.gov/srtm/index.html

Karig, D.E. & Kozlu, H. 1990. Late Palaeogene–Neogene evolution of the triple junction near Maraş, south-central Turkey. *Journal of the Geological Society, London*, **147**, 1023–1034.

Klinger, Y., Avouac, J.P., Abou Karaki, N., Dorbath, L., Bourles, D. & Reyss, J.L. 2000. Slip rate on the Dead Sea transform fault in northern Arava Valley (Jordan). *Geophysical Journal International*, **142**, 755–768.

Kroon, D., Alexander, I., Little, M., Lourens, L.J., Matthewson, A., Robertson, A.H.F. & Sakamoto, T. 1998. Oxygen isotope and sapropel stratigraphy in the Eastern Mediterranean during the last 3.2 million years. *In:* Robertson, A.H.F., Emeis, K.-C., Richter, C. & Camerlenghi, A. (eds) *Proceedings of the Ocean Drilling Program, Scientific Results, 160*. Ocean Drilling Program, College Station, TX, 181–189.

Kukla, G.J. 1975. Loess stratigraphy of central Europe. *In:* Butzer, K.W. & Isaac, G.L. (eds) *After the Australopithecines*. Mouton, The Hague, 99–188.

Kukla, G.J. 1978. The classical European glacial stages: correlation with deep-sea sediments. *Transactions of the Nebraska Academy of Sciences*, **6**, 57–93.

Kuzcuoğlu, C., Fontugne, M. & Mouralis, D. 2004. Holocene terraces in the Middle Euphrates valley between Halfeti and Karkemish (Gaziantep, Turkey).

Downloaded from http://jgs.lyellcollection.org/ at University of St Andrews on February 27, 2015

Quaternaire, **15**, 195–206.

Lyberis, N., Yürür, T., Chorowicz, J., Kasapoğlu, E. & Gündoğdu, N. 1992. The East Anatolian fault: an oblique collisional belt. *Tectonophysics*, **204**, 1–15.

McClusky, S., Balassanian, S. & Barka, A. *et al*. 2000. Global Positioning System constraints on plate kinematics and dynamics in the eastern Mediterranean and Caucasus. *Journal of Geophysical Research*, **105**, 5695–5719.

McKenzie, D.P. 1976. The East Anatolian Fault: a major structure in eastern Turkey. *Earth and Planetary Science Letters*, **29**, 189–193.

Minzoni-Deroche, A. & Sanlaville, P. 1988. Le Paléolithique Inférieur de la région de Gaziantep. *Paléorient*, **14**, 87–98.

Muehlberger, R.W. 1981. The splintering of the Dead Sea Fault Zone in Turkey. *Yerbilimleri*, **8**, 123–130.

Muehlberger, R.W. & Gordon, M.B. 1987. Observations on the complexity of the East Anatolian Fault, Turkey. *Journal of Structural Geology*, **9**, 899–903.

Perinçek, D. & Kozlu, H. 1983. Stratigraphy and structural relations of the units if the Afşin–Elbistan–Doğanşehir region (eastern Taurus). *In:* Tekeli, O. & Göncüoğlu, M.C. (eds) *Geology of the Taurus Belt. Proceedings of the 1983 Ankara Symposium*. General Directorate of Mineral Research and Exploration, Ankara, 181–198.

Ponikarov, V.P., Kazmin, V.G., Mikhailov, I.A., *et al*. 1967. *The Geology of Syria: Explanatory Notes on the Geological Map of Syria, Scale 1:500 000. Part I: Stratigraphy, Igneous Rocks, and Tectonics*. Vsesoj. Exportno-Import Objed. Technoexport, Moscow; Ministry of Industry, Syrian Arab Republic, Damascus.

Rohling, E.J. & Hilgen, F.J. 1991. The eastern Mediterranean climate at times of sapropel formation: a review. *Geologie en Mijnbouw*, **70**, 253–264.

Rossignol-Strick, M. 1985. Mediterranean Quaternary sapropels, an immediate response of the African monsoon to variations of insolation. *Palaeogeography, Palaeoclimatology, Palaeoecology*, **49**, 237–263.

Rossignol-Strick, M. 1999. The Holocene climatic optimum and pollen records of sapropel 1 in the eastern Mediterranean, 9000–6000 BP. *Quaternary Science Reviews*, **18**, 515–530.

Şaroğlu, F., Emre, Ö. & Kuşçu, İ. 1992. The East Anatolian fault zone of Turkey. *Annales Tectonicae*, **6**, 99–125.

Shackleton, N.J., Berger, A. & Peltier, W.R. 1990. An alternative astronomical calibration of the Lower Pleistocene timescale based on ODP site 677. *Transactions of the Royal Society of Edinburgh*, **81**, 252–261.

Terlemez, H.C., Şentürk, K., Ateş, Ş. & Oral, A. 1997. *Geological map of the Gaziantep-K24 quadrangle, 1:100 000 scale, and accompanying 18 page explanatory booklet*. General Directorate of Mineral Research and Exploration, Ankara.

Tolun, N. & Erentöz, C. 1962. *Hatay sheet of the Geological Map of Turkey, 1:500 000 scale*. General Directorate of Mineral Research and Exploration, Ankara.

Tyráček, J. 1987. Terraces of the Euphrates River. *Sborník geologických Věd, Antropozoikum*, **18**, 185–202.

Westaway, R. 1994. Present-day kinematics of the Middle East and eastern Mediterranean. *Journal of Geophysical Research*, **99**, 12071–12090.

Westaway, R. 1995. Deformation around stepovers in strike-slip fault zones. *Journal of Structural Geology*, **17**, 831–847.

Westaway, R. 2001. Flow in the lower continental crust as a mechanism for the Quaternary uplift of the Rhenish Massif, north-west Europe. *In:* Maddy, D., Macklin, M. & Woodward, J. (eds) *River Basin Sediment Systems: Archives of Environmental Change*. Balkema, Rotterdam, 87–167.

Westaway, R. 2002a. The Quaternary evolution of the Gulf of Corinth, central Greece: coupling between surface processes and flow in the lower continental crust. *Tectonophysics*, **348**, 269–318.

Westaway, R. 2002b. Geomorphological consequences of weak lower continental crust, and its significance for studies of uplift, landscape evolution, and the interpretation of river terrace sequences. *Netherlands Journal of Geosciences*, **81**, 283–304.

Westaway, R. 2002c. Long-term river terrace sequences: evidence for global increases in surface uplift rates in the Late Pliocene and early Middle Pleistocene caused by flow in the lower continental crust induced by surface processes. *Netherlands Journal of Geosciences*, **81**, 305–328.

Westaway, R. 2003. Kinematics of the Middle East and Eastern Mediterranean updated. *Turkish Journal of Earth Sciences*, **12**, 5–46.

Westaway, R. 2004a. Kinematic consistency between the Dead Sea Fault Zone and the Neogene and Quaternary left-lateral faulting in SE Turkey. *Tectonophysics*, **391**, 203–237.

Westaway, R. 2004b. Comment on 'Late Cenozoic reorganization of the Arabia–Eurasia collision and the comparison of short-term and long-term deformation rates' by M. Allen, J. Jackson, and R. Walker. *Tectonics*, **23**(TC5006), doi:10.1029/2004TC001674 (published online).

Westaway, R. & Arger, J. 1996. The Gölbaşı basin, southeastern Turkey: a complex discontinuity in a major strike-slip fault zone. *Journal of the Geological Society, London*, **153**, 729–743.

Westaway, R. & Arger, J. 2001. Kinematics of the Malatya–Ovacık Fault Zone. *Geodinamica Acta*, **14**, 103–131.

Westaway, R., Pringle, M., Yurtmen, S., Demir, T., Bridgland, D., Rowbotham, G. & Maddy, D. 2004. Pliocene and Quaternary regional uplift in western Turkey: the Gediz river terrace staircase and the volcanism at Kula. *Tectonophysics*, **391**, 121–169.

Westaway, R., Bridgland, D. & White, M. 2005. The Quaternary uplift history of central southern England: evidence from the terraces of the Solent River system and nearby raised beaches. *Quaternary Science Reviews*, in press.

Wilkinson, T.J. 1990. *Town and Country in Southeastern Anatolia. I: Settlement and Land Use at Kurban Höyük and Other Sites in the Lower Karababa Basin*. University of Chicago Oriental Institute Publications, **109**.

Yalçin, N. 1979. Doğu Anadolu yarılımının Türkoğlu–Karaağaç (K. Maraş) arasındakı kesiminin özellikleri ve bölgedeki yerleşim alanları. *In: TJK Altınlı Simpozyumu Bildiriler Kitabı*. Türkiye Jeoloji Kurumu, Ankara, 49–56.

Yurtmen, S., Guillou, H., Westaway, R., Rowbotham, G. & Tatar, O. 2002. Rate of strike-slip motion on the Amanos Fault (Karasu Valley, southern Turkey) constrained by K–Ar dating and geochemical analysis of Quaternary basalts. *Tectonophysics*, **344**, 207–246.

Yürür, M.T. & Chorowicz, J. 1998. Recent volcanism, tectonics and plate kinematics near the junction of the African, Arabian and Anatolian plates in the eastern Mediterranean. *Journal of Volcanology and Geothermal Research*, **85**, 1–15.

Received 21 February 2005; revised typescript accepted 19 July 2005.
Scientific editing by Tim Needham